ENGINEERING GLUCOSE TOLERANCE IN β-GLUCOSIDASE AND APPLICATION IN BIOFUEL CELLS

LUCIRANON SRIBRAHMA

A Thesis Submitted in Fulfillment of the Requirements for the
Degree of Master of Science in Biochemistry and Biochemical Technology
Suranaree University of Technology
Academic Year 2024

วิศวกรรมความทนทานต่อกลูโคสในเอนไซม์เบต้า-กลูโคซิเดส และการประยุกต์ใช้ในเซลล์เชื้อเพลิงชีวภาพ

นายลุศิราณณพ์ ศรีพรหม

วิทยานิพนธ์นี้สำหรับการศึกษาตามหลักสูตรปริญญาวิทยาศาสตรมหาบัณฑิต
สาขาวิชาชีวเคมีและเทคโนโลยีชีวเคมี
มหาวิทยาลัยเทคโนโลยีสุรนารี
ปีการศึกษา 2567

ENGINEERING GLUCOSE TOLERANCE IN β-GLUCOSIDASE AND APPLICATION IN BIOFUEL CELLS

Suranaree University of Technology has approved this thesis submitted in partial fulfillment of the requirements for a Master's degree.

Thesis Examining Committee

(Asst. Prof. Dr. Thanyaporn Wongnate)
Chairperson

(Prof. Dr. James R. Ketudat-Cairns)
Member (Thesis Advisor)

(Asst. Prof. Dr. Piyanut Pinyou)
Member (Thesis Co-advisor)

(Assoc. Prof. Dr. Panida Khunkaewla)
Member

(Assoc. Prof. Dr. Jaruwan Siritapetawee)
Member

(Assoc. Prof. Dr. Yupaporn Ruksakulpiwat)
Acting Vice Rector for Academic Affairs and Quality Assurance

(Prof. Dr. Santi Maensiri)
Acting Dean of Institute of Science

ลุศิราณณพ์ ศรีพรหม : วิศวกรรมความทนทานต่อกลูโคสในเอนไซม์เบต้า-กลูโคซิเดสและการประยุกต์ใช้ในเซลล์เชื้อเพลิงชีวภาพ (ENGINEERING GLUCOSE TOLERANCE IN β-GLUCOSIDASE AND APPLICATION IN BIOFUEL CELLS). อาจารย์ที่ปรึกษา : ศาสตราจารย์ ดร.เจมส์ เกตุทัต-คาร์นส์ และ อาจารย์ที่ปรึกษาร่วม : ผู้ช่วยศาสตราจารย์ ดร.ปิยะนุช ปิ่นอยู่, 70 หน้า.

คำสำคัญ : เซลล์เชื้อเพลิงชีวมวล, วิศวกรรมเอนไซม์, เบต้า-กลูโคซิเดส, กลูโคสดีไฮโดรจีเนสที่ต้องอาศัย FAD ในการทำงาน, ความไม่ไวต่อออกซิเจน

ความต้องการที่เพิ่มขึ้นต่อแหล่งพลังงานทดแทนและยั่งยืนได้กระตุ้นให้เกิดนวัตกรรมในเทคโนโลยีเซลล์เชื้อเพลิงจากชีวมวล งานวิจัยนี้รายงานการพัฒนาเซลล์เชื้อเพลิงชีวมวลที่มีประสิทธิภาพสูงและไม่ไวต่อออกซิเจน โดยอาศัยวิศวกรรมเอนไซม์และกลยุทธ์ทางเคมีไฟฟ้าขั้นสูง การออกแบบแอโนดใช้เอนไซม์ที่ทำงานร่วมกัน ได้แก่ เบต้า-กลูโคซิเดส (β-glucosidase, BGL5) จาก *Agrobacterium tumefaciens* และเอนไซม์กลูโคส ดีไฮโดรจีเนสที่ต้องอาศัย FAD ในการทำงาน (FAD-GlcDH) จาก *Talaromyces emersonii* ทั้งสองเอนไซม์ถูกแสดงออกใน Escherichia coli โดยใช้เวกเตอร์ pET30a และ pET32a การวิเคราะห์สมบัติทางจลนพลศาสตร์แสดงให้เห็นถึงประสิทธิภาพการเร่งปฏิกิริยาที่สูง: BGL5 มีค่าคงที่ทางจลนศาสตร์ของเอนไซม์ (K_m) 0.17 มิลลิโมลาร์ และ ค่าอัตราสูงสุดของปฏิกิริยาที่เร่งด้วยเอนไซม์ (V_{max}) 283 ไมโครโมลต่อนาทีต่อมิลลิกรัมโดยใช้พารา-ไนโตรฟีนิล-เบต้า-ดี-กลูโคไพราโนไซด์ (*p*NPG) เป็นสับสเตรทขณะที่ FAD-GlcDH มีค่า K_m 411 มิลลิโมลาร์ และ V_{max} 7040 ไมโครโมลต่อนาทีต่อมิลลิกรัมโดยใช้กลูโคสเป็นสับสเตรท การทำให้ BGL5 กลายพันธุ์แบบมีเป้าหมาย (H229S) แสดงความสามารถในการทนต่อกลูโคสได้ดีขึ้นอย่างมีนัยสำคัญ โดยมีค่า IC50 1320 มิลลิโมลาร์ เทียบกับ 94 มิลลิโมลาร์ของเอนไซม์ชนิดดั้งเดิม ระบบเคมีไฟฟ้าถูกประกอบขึ้นโดยใช้ BGL5 ชนิดดั้งเดิมในสารละลายเซลโลไบโอส ที่ pH 7.0 ร่วมกับการตรึงเอนไซม์ GlcDH, พอลิเอทิลีนอิมีน-เฟอร์โรซีน (PEI-Fc) และโพลีเอทิลีนไกลคอล ไดไกลซิดิลอีเทอร์ (PEGDGE) บนอิเล็กโทรดกราฟีน เซลโลไบโอสจะถูก BGL5 เร่งการย่อยสลายด้วยน้ำเป็นกลูโคส 2 โมเลกุล ซึ่งต่อมาจะถูก GlcDH ออกซิไดซ์เป็นกลูโคโนแลคโตน โดยมี PEI-Fc ทำหน้าที่เป็นตัวกลางถ่ายอิเล็กตรอนระหว่างเทอจีดีเอชกับผิวอิเล็กโทรด ทางด้านแคโทด ฮอร์สแรดิช เปอร์ออกซิ-

เดส (HRP) ถูกตรึงแบบโคเวเลนต์ผ่านสาร 1-ไพรีนบิวทาโนอิก แอซิด ซัคซินิไมดิล เอสเทอร์ (PBSE) ทำให้สามารถเกิดการซ้อนทับแบบไพ-ไพ (π-π stacking) กับอิเล็กโทรดโพลีอิ-ไมด์เคลือบกราฟีน โครงสร้างนี้ถูกทำให้เสถียรเพิ่มเติมด้วย Nafion™ ความเข้มข้น 0.5% เพื่อให้การรีดักชันของไฮโดรเจนเปอร์ออกไซด์เป็นไปอย่างมีประสิทธิภาพ โดยใช้ 2,2′-azinobis (3-ethylbenzothiazoline-6-sulfonic acid) ammonium salt; (AzBTS) เป็นตัวกลางรี-ดอกซ์ โครงสร้างของเซลล์เชื้อเพลิงชีวภาพนี้สามารถให้ความหนาแน่นกำลังไฟสูงสุดที่ 126 ไมโครวัตต์ต่อตารางเซนติเมตร และแรงดันวงจรเปิดที่ 0.6 โวลต์ อาจเพียงพอสำหรับจ่ายพลังงานให้กับอุปกรณ์อิเล็กทรอนิกส์พลังงานต่ำ ความไม่ไวต่อออกซิเจนและประสิทธิภาพการเร่งปฏิกิริยาที่สูงของระบบนี้ถือเป็นก้าวสำคัญสู่การประยุกต์ใช้งานจริงของระบบพลังงานชีวไฟฟ้าเคมี ผลการวิจัยนี้เน้นย้ำถึงศักยภาพของเซลล์เชื้อเพลิงชีวมวลที่ใช้เอนไซม์ที่ผ่านการดัดแปลงและพื้นผิวกราฟีนในการพัฒนาเทคโนโลยีพลังงานอย่างยั่งยืนในอนาคต

สาขาวิชาเคมี
ปีการศึกษา 2567

ลายมือชื่อนักศึกษา _____
ลายมือชื่ออาจารย์ที่ปรึกษา _____
ลายมือชื่ออาจารย์ที่ปรึกษาร่วม Piyanut Pinyou

LUCIRANON SRIBRAHMA : ENGINEERING GLUCOSE TOLERANCE IN β-GLUCOSIDASE AND APPLICATION IN BIOFUEL CELLS. THESIS ADVISOR : PROF. JAMES R. KETUDAT-CAIRNS, Ph.D. AND THESIS CO-ADVISOR : ASST. PROF. PIYANUT PINYOU, Ph.D. 70 PP.

Keywords: Biomass fuel cell, Enzyme engineering, β-glucosidase (BGL5), FAD-dependent glucose dehydrogenase (FAD-GDH), Oxygen-insensitive

The increasing demand for renewable and sustainable energy sources has spurred innovations in biomass fuel cell technologies. This study reports the development of a high-efficiency, oxygen-insensitive biomass fuel cell through enzyme engineering and advanced electrochemical strategies. The anode design utilizes a synergistic enzyme pair: β-glucosidase (BGL) from *Agrobacterium tumefaciens* (BGL5, GH1 family) and FAD-dependent glucose dehydrogenase (FAD-GlcDH) from *Talaromyces emersonii*. Both enzymes were heterologously expressed in *Escherichia coli* using pET30a and pET32a vectors. Kinetic characterization revealed high catalytic efficiencies: BGL5 exhibited a K_m of 0.17 mM and V_{max} of 283 μmol/min·mg for *p*NPG, while FAD-GDH showed a K_m of 411 mM and V_{max} of 7040 μmol/min·mg for glucose. A rationally engineered BGL5 mutant (H229S) demonstrated significantly improved glucose tolerance, with an IC50 of 1320 mM compared to 94 mM for the wild type. The electrochemical system was assembled with wild-type BGL in the cellobiose solution, pH 7.0, with immobilized GlcDH, polyethyleneimine-ferrocene (PEI-Fc), and Poly(ethylene glycol) diglycidyl ether (PEGDGE) on a graphene electrode. Cellobiose is hydrolyzed by BGL into two molecules of D-glucose, which are subsequently oxidized to gluconolactone by TeGlcDH, with PEI-Fc facilitating mediated electron transfer between TeGlcDH and the electrode surface. On the cathode side, horseradish

peroxidase (HRP) was covalently immobilized via 1- pyrenebutanoic acid succinimidyl ester (PBSE), enabling π-π stacking on a graphene-coated polyimide electrode. The configuration was further stabilized with 0.5% Nafion, enabling efficient hydrogen peroxide reduction using 2,2′-azinobis(3-ethylbenzothiazoline-6-sulfonic acid) ammonium salt (AzBTS) as a redox mediator. This biofuel cell configuration achieved a maximum power density of 126 μW/cm² with an open-circuit voltage of 0.6 V, which may be sufficient to power low-energy electronic devices. The system's oxygen insensitivity and high catalytic performance make it a significant step toward practical applications of bioelectrochemical energy systems. These findings highlight the potential for enzyme-engineered, graphene-based biomass fuel cells in the future of sustainable energy technologies.

School of Chemistry
Academic Year 2024

Student's Signature _____
Advisor's Signature _____
Co-advisor's Signature Piyanut Pinyou

ACKNOWLEDGEMENTS

I would like to express my sincere gratitude to Prof. Dr. James R. Ketudat-Cairns and Asst. Prof. Dr. Piyanut Pinyou, my thesis advisors, for their patience, invaluable guidance, unwavering support, insightful discussions, and continuous encouragement throughout the course of my research. In addition, I am deeply thankful to Asst. Prof. Dr. Thanyaporn Wongnate, Assoc. Prof. Dr. Panida Khunkaewla, and Assoc. Prof. Dr. Jaruwan Siritapetawee for serving as members of my thesis examination committee and for their constructive feedback and contributions. I gratefully acknowledge the Development and Promotion of Science and Technology Talents Project (DPST), Thailand, for the generous scholarship support during my master's studies, and Suranaree University of Technology (SUT) for providing the resources and environment necessary for my academic development. A special thanks goes to Ms. Chamaipon Beagbandee for her valuable suggestions on research methodology and for conducting the cloning of the H229S mutant used in this study. Finally, I am profoundly grateful to my family for their unconditional love, support, and encouragement throughout this journey.

Luciranon Sribrahma

CONTENTS

CONTENTS (Continued)

LIST OF TABLES

Table **Page**

LIST OF FIGURES

Figure **Page**

LIST OF FIGURES (Continued)

Figure **Page**

LIST OF ABBREVIATIONS

1-mPMS	1-Methoxy-5-methylphenazinium methyl sulfate
AtBGL	beta-glucosidase from *Agrobacterium Tumefaciens*
AzBTS	2,2'-Azino-bis (3-ethylbenzothiazoline-6-sulfonic acid)
CNT	carbon nanotube
CV	cyclic voltammetry
DCPIP	2,6-Dichlorophenolindophenol
DET	direct electron transfer
EIS	Electro impedance spectroscopy
FAD	Flavin Adenine Dinucleotide
GDL	Glucono-δ-lactone
Glc	Glucose
GOx	glucose oxidase
H229S	Mutant form of β-glucosidase with histidine at position 229 replaced by serine
HRP	horseradish peroxidase
IC50	Half maximal inhibitory concentration
IMAC	Immobilized Metal Affinity Chromatography
IPTG	Isopropyl β-D-thiogalactopyranoside
Kcat	catalytic constant of the enzyme
Kcat/Km	enzyme efficiency value
kDa	kilodalton
K_i	inhibition constant
K_{ic}	competitive inhibition constant
K_{iu}	uncompetitive inhibition constant
K_m	Michaelis-Menten constant
MET	mediated electron transfer
min	minute

LIST OF ABBREVIATIONS (Continued)

NaCl	sodium chloride
nm	nanometer
O/N	overnight
OCP	open circuit potential
PBS	phosphate buffer saline
PBSE	1-Pyrenebutyric acid N-hydroxysuccinimide ester
PEGDGE	Poly(ethylene glycol) diglycidyl ether
PEI-Fc	polyethyleneimine-ferrocene
pH	Potential of Hydrogen
pNPGlc	para-Nitro-phenyl-β-D-Glucopyranoside
pPET(30, 32)	plasmid for Expression by T7 RNA polymerase, 30 and 32 series
rpm	round per minute
SDS-PAGE	sodium dodecyl sulfate polyacrylamide gel electrophoresis
TeGlcDH	Glucose dehydrogenase from *Talaromyces emersonii*
v/v	volume by volume
V_{max}	maximum velocity of the enzyme
w/v	weight by volume

CHAPTER I

INTRODUCTION

1.1 Rationale of this study

Global warming is a major crisis driven by greenhouse gas emissions, deforestation, and unsustainable energy use. As industrialization accelerates, fossil fuels remain a leading cause of environmental degradation. The urgent need for sustainable, carbon-neutral energy solutions calls for innovative technologies to curb emissions and reshape energy production.

Biomass fuel cells offer a promising alternative by converting organic materials into electricity through enzymatic reactions, unlike traditional combustion-based methods. Utilizing non-edible biomass, such as agricultural waste and forestry residues, they provide a continuous power source independent of weather conditions while reducing waste and pollution (Moradian et al., 2021). D-Gluconic acid, produced via glucose oxidation and hydrolytic ring opening of D-glucono-δ-lactone, has a growing demand in industries like food, cosmetics, and agriculture (F. Kornecki et al., 2020; *Gluconic Acid - an Overview | ScienceDirect Topics*, n.d.). Glucose fuel cells (GFCs) could contribute to sustainable development by generating energy while producing D-glucono-δ-lactone, which hydrolyzes to D-gluconic acid. However, both biological and chemical fuel cells face commercialization challenges, including high costs and material limitations. Many current catalysts rely on expensive precious metals like platinum and gold, and enzymatic fuel cells suffer from low power density due to slow electron transfer. (Barelli et al., 2021).

Our project aims to leverage protein engineering and electrochemistry to enhance biomass fuel cell performance. We propose using β-glucosidase (BGL) and FAD-dependent glucose dehydrogenase (FAD-GDH) to generate electricity from biomass-derived gluco-oligosaccharides. BGL hydrolyzes ß-glycosidic bonds to release glucose, while FAD-GDH oxidizes glucose to D-glucono-δ-lactone without oxygen interference. The combination of BGL and FAD-glucose dehydrogenase is part of the anode, and the cathode of the biofuel cell is the combination of horseradish peroxidase (HRP) the hydrogen peroxide is catalyzed by the HRP to water molecules. This catalytic conversion requires electrons to reduce H_2O_2 to a water molecule, which is appropriate for the cathode.

A key challenge is BGL inhibition by its product, D-glucose, and D-glucono-δ-lactone, the product of glucose dehydrogenase and glucose oxygenase. Our project seeks to engineer BGL for improved glucose tolerance by testing previously reported glucose-insensitive mutant enzymes to see whether they enhance its efficiency for electricity generation.

1.2 Objective

The objectives of this research include

1) To produce a glucose-tolerant β-glucosidase and assess its benefit for an anode generating electrons from biomass-derived glucose.
2) To produce an oxygen-insensitive glucose dehydrogenase and assess its benefit for the anode-generating electrons from biomass-derived glucose.
3) To combine the glucose dehydrogenase and β-glucosidase for current generation from a biomass digest and assess the relative benefits compared to a system with glucose-sensitive ß-glucosidase and glucose oxidase.

1.3 References

Barelli, L., Bidini, G., Pelosi, D., and Sisani, E. (2021). Enzymatic Biofuel Cells: A Review on Flow Designs. *Energies*, *14*(4), Article 4.

F. Kornecki, J., Carballares, D., W. Tardioli, P., C. Rodrigues, R., Berenguer-Murcia, Á., R. Alcántara, A., and Fernandez-Lafuente, R. (2020). Enzyme production of d -gluconic acid and glucose oxidase: Successful tales of cascade reactions. *Catalysis Science & Technology*, *10*(17), 5740–5771.

Gluconic Acid—An overview | ScienceDirect Topics. (n.d.). Retrieved June 11, 2024, from www.sciencedirect.com/topics/biochemistry-genetics-and-molecular-biology/gluconic-acid

Moradian, J. M., Fang, Z., and Yong, Y.-C. (2021). Recent advances on biomass-fueled microbial fuel cell. *Bioresources and Bioprocessing*, *8*(1), 14.

CHAPTER II

LITERATURE REVIEW

2.1 Glycoside hydrolases and β-Glucosidase

Glycoside hydrolases (GHs) are a broad class of enzymes that catalyze the hydrolysis of glycosidic bonds in carbohydrates and glycoconjugates. These enzymes are classified into distinct families based on amino acid sequence similarity, structural features, and catalytic mechanisms, as curated in the CAZy (Carbohydrate-Active enZymes) database (www.cazy.org; Drula et al., 2022). Each GH family typically shares a conserved protein fold and catalytic machinery, although substrate specificity and biological function can vary widely.

Within this diverse enzyme class, β-glucosidases (β-D-glucopyranoside glucohydrolases, EC 3.2.1.21) represent a well-studied group that catalyzes the hydrolysis of glycosidic bonds to release non-reducing terminal glucosyl residues from glycosides and oligosaccharides. These enzymes are ubiquitous in nature present in Archaea, Eubacteria, and Eukaryotes and play crucial biological roles, including biomass degradation in microorganisms, glycolipid metabolism in animals, and cell wall lignification, defense responses, and hormone activation in plants (Ketudat Cairns and Esen, 2010). Although β-glucosidases occur in several GH families, the catalytic domain typically adopts a conserved structural fold within each family, some of which are related to each other (Figure 2.3).

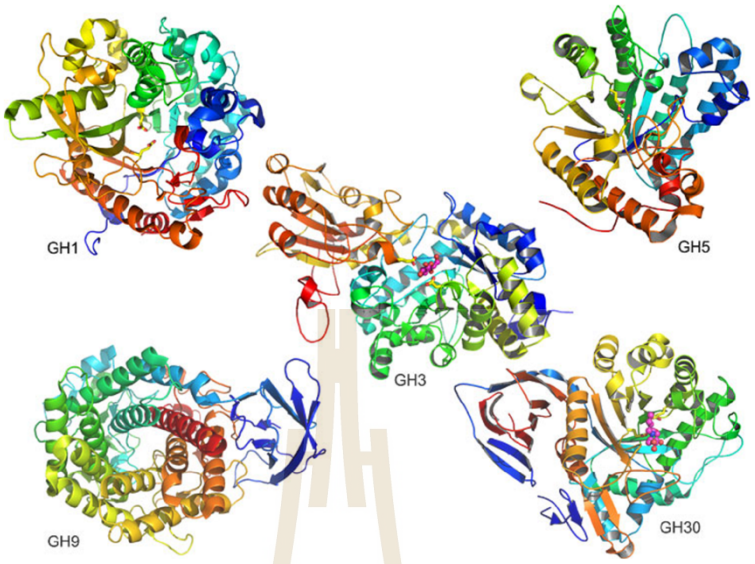

Figure 2.1 Structures of β-glucosidases from different GH families.

Mechanism of Action

β-Glucosidases catalyze the hydrolysis of β-glucosidic linkages and typically operate via either a retaining or an inverting mechanism, depending on the enzyme class. The retaining mechanism, which is commonly observed in glycoside hydrolase families such as GH1 and GH3, proceeds via a two-step double-displacement reaction involving a covalent glycosyl-enzyme intermediate. This process is facilitated by two critical acidic amino acid residues, usually glutamates or aspartates. One residue functions as a nucleophile, while the other acts as a general acid/base catalyst.

In the first step, known as glycosylation, the substrate binds to the active site, positioning the glycosidic bond for cleavage. The nucleophilic glutamate attacks the anomeric carbon of the sugar, resulting in the departure of the aglycone moiety and the formation of a covalent glycosyl-enzyme intermediate. Simultaneously, the acid/base catalyst donates a proton to the glycosidic oxygen, promoting aglycone release. In the second step, deglycosylation, a water molecule is activated by the same acid/base glutamate and then attacks the glycosyl-enzyme intermediate. This leads to the hydrolysis of the intermediate, releasing the glucose product and regenerating the

free enzyme. This mechanism retains the configuration of the anomeric carbon between the substrate and product.

In contrast, the inverting mechanism, employed by other glycosidase families, proceeds through a single-step direct displacement reaction and does not involve a covalent intermediate. Instead, two acidic residues act simultaneously: one as a general acid to protonate the glycosidic oxygen, and the other as a general base to activate a water molecule for nucleophilic attack on the anomeric carbon. This results in the direct displacement of the aglycone and the inversion of the stereochemistry at the anomeric center in the product relative to the substrate.

Understanding whether a β-glucosidase follows a retaining or inverting mechanism provides critical insight into its catalytic strategy, potential substrate specificity, and implications for enzyme engineering and inhibitor design.

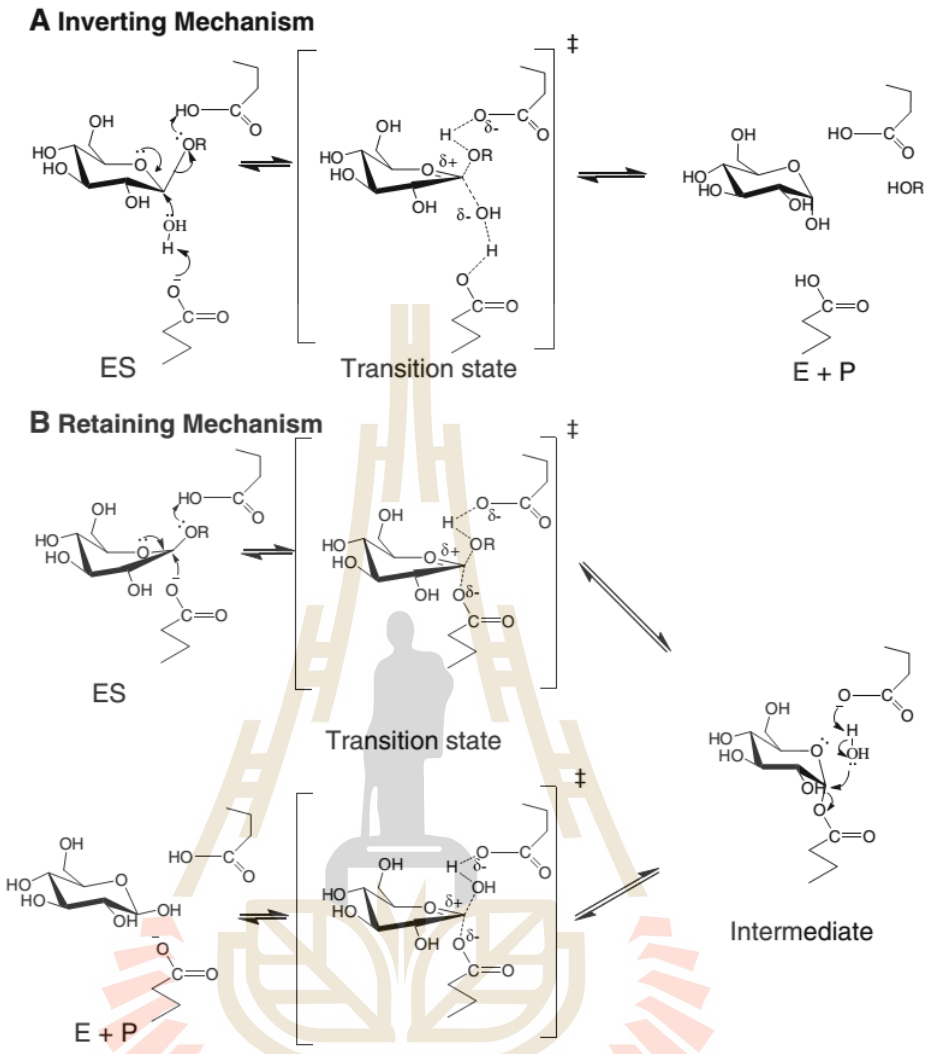

Figure 2.2 Catalytic mechanisms of inverting and retaining β-glucosidases(Ketudat Cairns and Esen, 2010).

Applications in Biotechnology

β-Glucosidases (EC 3.2.1.21) are versatile enzymes with significant industrial applications across various sectors. In the biofuel industry, they play a crucial role in the enzymatic hydrolysis of lignocellulosic biomass by catalyzing the final step of cellulose degradation, converting cellobiose into glucose—which is essential for efficient bioethanol production. Their ability to function under diverse conditions

makes them valuable in enhancing the saccharification process, thereby improving the overall yield of fermentable sugars (Badoni et al., 2025).

In the food and beverage industry, β-glucosidases are employed to enhance flavors and aromas. In winemaking, these enzymes hydrolyze glycosidic bonds in aroma precursors, releasing volatile compounds such as terpenes, which contribute to the varietal aroma and flavor complexity of wines. Similarly, in fruit juice processing, β-glucosidases can liberate aromatic compounds from glycosidic precursors, enriching the flavor profile of beverages like passion fruit juice (Gao et al., 2022; Maicas and Mateo, 2016; Romo-Sánchez et al., 2014; Zhang et al., 2021).

In animal feed production, β-glucosidases are utilized to improve the nutritional value of feedstocks. By breaking down anti-nutritional factors such as cyanogenic glycosides and releasing glucose from complex carbohydrates, these enzymes enhance the digestibility and energy content of feeds, leading to better animal growth and health (Singh et al., 2016).

The pharmaceutical industry also benefits from β-glucosidase applications. These enzymes are involved in the bioconversion of glycosylated compounds into their active aglycone forms, which often exhibit enhanced bioavailability and therapeutic efficacy. For instance, β-glucosidases are used in the synthesis of bioactive compounds and in the modification of natural products to develop novel pharmaceuticals (Tran et al., 2023).

Overall, the multifunctional nature of β-glucosidases and their ability to act on a wide range of substrates under various conditions underscore their industrial significance. Ongoing research and development continue to explore and expand their applications, aiming to optimize processes and develop innovative solutions across multiple industries.

2.2 Flavin Adenine Dinucleotide-dependent Glucose Dehydrogenase (FAD-GDH)

FAD-dependent glucose dehydrogenase (FAD-GDH) represents a compelling subject of study in the field of bioelectrochemistry and biosensor technology, due to its unique electron transfer mechanism, oxygen insensitivity, and potential for bioelectronic integration. This enzyme catalyzes the oxidation of β-D-glucose to D-glucono-1,5-lactone while reducing the flavin adenine dinucleotide (FAD) cofactor. Unlike the more traditional glucose oxidase (GOx), which transfers electrons via molecular oxygen and produces hydrogen peroxide, FAD-GDH utilizes direct or mediated electron transfer pathways, making it more suitable for applications where oxygen interference or peroxide accumulation poses a problem, such as in continuous glucose monitoring (Okuda-Shimazaki et al., 2020).

At the heart of FAD-GDH's functionality lies its redox-active FAD cofactor, covalently or non-covalently bound within the enzyme's active site. Upon substrate binding, glucose donates electrons to FAD, reducing it to $FADH_2$. These electrons then need to be transferred to an external electron acceptor, a process that defines the enzyme's operational efficiency in bioelectronic systems (Figure 2.3). Depending on the organismal origin and isoform, this transfer can occur via direct electron transfer (DET), where electrons move directly from the reduced cofactor to the electrode surface, or via mediated electron transfer (MET), which involves small redox-active compounds shuttling electrons from the enzyme to the electrode. In most fungal and bacterial FAD-GDHs, MET is the more prominent pathway, as the enzyme's FAD cofactor is often buried within the protein matrix, limiting surface access to the electrode.

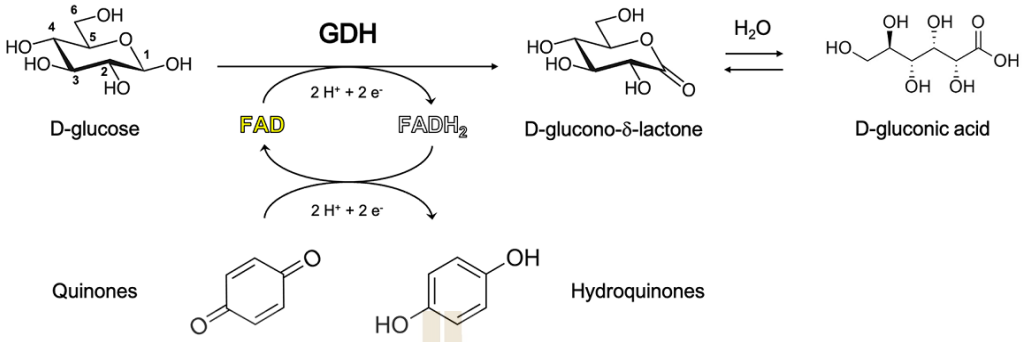

Figure 2.3 Catalytic mechanism of glucose dehydrogenases (GDHs) (Cerutti et al., 2021).

Structurally, FAD-GDHs exhibit diversity based on their phylogenetic origins. Fungal FAD-GDHs (fFAD-GDHs) are typically monomeric enzymes with a tightly bound FAD cofactor, whereas bacterial FAD-GDHs (bFAD-GDHs) often consist of multiple subunits, including cytochrome domains that facilitate direct electron transfer (DET). This structural variability influences their electron transfer capabilities and suitability for integration into biosensor platforms (Okuda-Shimazaki et al., 2020).

A key advantage of FAD-GDH over GOx is its oxygen independence (Okuda-Shimazaki et al., 2020). While GOx activity depends on molecular oxygen as the electron acceptor—thus susceptible to fluctuations in local oxygen concentration—FAD-GDH uses alternative electron acceptors, which can be synthetic redox mediators or conductive electrodes. This characteristic makes FAD-GDH an ideal candidate for continuous glucose monitoring systems (CGMs), where oxygen levels can vary across physiological environments and measurement conditions. Moreover, this trait eliminates the production of hydrogen peroxide, which is not only potentially harmful but also complicates signal interpretation in amperometric biosensors.

Another fascinating aspect of FAD-GDH is the breadth of its electron mediator compatibility (Okuda-Shimazaki et al., 2020). The enzyme has been shown to function efficiently with a range of redox mediators, such as phenazine methosulfate (PMS), 1-methoxy-5-methylphenazinium methyl sulfate (1-mPMS), and various ferrocene

derivatives. These mediators play a critical role in MET-based sensor systems, ensuring rapid electron transfer kinetics and enhanced signal stability. The selection of an appropriate mediator affects not only the sensitivity and response time of the biosensor but also its long-term stability and biocompatibility, especially in clinical or wearable applications.

Recent structural studies and protein engineering efforts have deepened the understanding of FAD-GDH's redox mechanism. Crystallographic and spectroscopic analyses have revealed insights into the active site geometry, the orientation of the FAD cofactor, and the possible electron transfer pathways within the protein scaffold (Komori et al., 2015). By introducing surface mutations or domain fusions (Algov et al., 2021)(Ito et al., 2021), researchers have been able to improve electron tunneling rates, alter substrate specificity, and increase thermal or pH stability (Hua et al., 2022). These modifications have expanded the utility of FAD-GDH in diverse biotechnological platforms from glucose biofuel cells to point-of-care diagnostic devices.

In conclusion, FAD-dependent glucose dehydrogenase stands out as a versatile redox enzyme, distinguished by its oxygen insensitivity, structural adaptability, and compatibility with both direct and mediated electron transfer modes. As advances in protein engineering, electrode surface chemistry, and biosensor miniaturization continue, FAD-GDH will likely remain a central player in the development of next-generation bioelectronic devices. Its role bridges fundamental redox enzymology and applied electrochemical technology, offering a powerful example of how nature's catalytic systems can be harnessed for modern analytical and energy solutions.

2.3 Protein engineering

Protein engineering has emerged as a transformative field, enabling the design and modification of proteins with tailored functionalities for diverse applications in medicine, industry, and research. Traditional approaches, such as rational design and directed evolution (Figure 2.4), have laid the groundwork for manipulating protein structures and functions. Rational design leverages detailed knowledge of protein structures to introduce specific mutations, enhancing properties like stability and activity. For instance, structure-guided modifications have been employed to improve enzyme performance by targeting active sites and flexible loops, thereby fine-tuning catalytic efficiency (Xu et al., 2023a) . Directed evolution, on the other hand, mimics natural selection by generating vast libraries of protein variants and selecting those with desired traits. This method has been instrumental in evolving enzymes with enhanced thermostability and altered substrate specificity (Xu et al., 2023a).

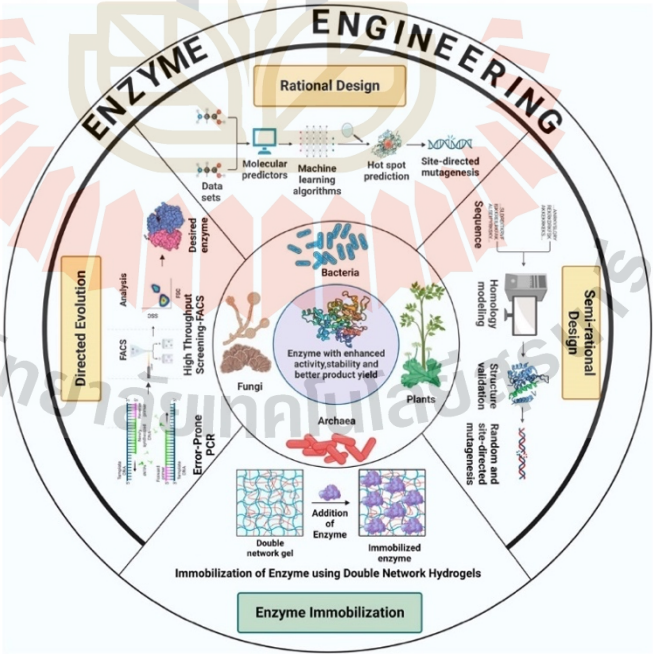

Figure 2.4 Schematic illustration of different strategies used for the improvement of catalytic properties and product yield of enzymes (Chatterjee et al., 2023).

The integration of computational tools has significantly advanced protein engineering. Machine learning (ML) models, trained on sequence-function data, have accelerated the prediction of beneficial mutations, reducing the experimental burden associated with traditional methods. ML-guided directed evolution combines the exploratory power of random mutagenesis with the precision of computational predictions, leading to more efficient protein optimization cycles (Xu et al., 2023b). Furthermore, the advent of deep learning models, such as AlphaFold, has revolutionized our ability to predict protein structures with remarkable accuracy, facilitating the rational design of proteins with novel functions (Qiu and Wei, 2023; Yang et al., 2019).

De novo protein design represents another frontier in the field, allowing the creation of entirely new protein structures not found in nature. Advancements in computational algorithms have enabled the design of proteins with specific geometries and functions, expanding the repertoire of available biomolecules for various applications. These designed proteins have potential uses ranging from therapeutic agents to industrial catalysts (Chen et al., 2022; Pan and Kortemme, 2021).

In industrial biotechnology, protein engineering has facilitated the development of enzymes with improved performance under harsh conditions, such as high temperatures and extreme pH levels. For example, engineered PETases have been optimized for enhanced degradation of polyethylene terephthalate (PET), contributing to sustainable plastic recycling efforts (Grigorakis et al., 2025). Additionally, the incorporation of non-canonical amino acids through expanded genetic codes has allowed the introduction of novel chemical functionalities into proteins, enabling the development of artificial metalloenzymes with unique catalytic properties (Wang et al., 2023).

The field has also seen the emergence of innovative techniques like *in situ* cyclization, which enhances protein stability by introducing covalent cross-links within the protein structure. This approach has proven effective in increasing the resilience of proteins under denaturing conditions, broadening their applicability in various biotechnological contexts (Neubacher et al., 2020)

Collectively, these advancements underscore the dynamic nature of protein engineering, where interdisciplinary approaches combining biology, chemistry, and computational science are driving the development of proteins with unprecedented capabilities. As the field continues to evolve, it holds immense promise for addressing complex challenges across multiple sectors.

2.4 Enzyme Immobilization

Enzyme immobilization is a pivotal technique in biotechnology and industrial applications, significantly enhancing the stability, reusability, and efficiency of enzymes. By anchoring enzymes onto various supports, the immobilization process addresses several limitations of free enzymes, such as their instability, difficulty in recovery, and high operational costs. The primary methods of enzyme immobilization include adsorption, covalent binding, entrapment, and encapsulation, each offering distinct advantages and challenges (Rana et al., 2022)

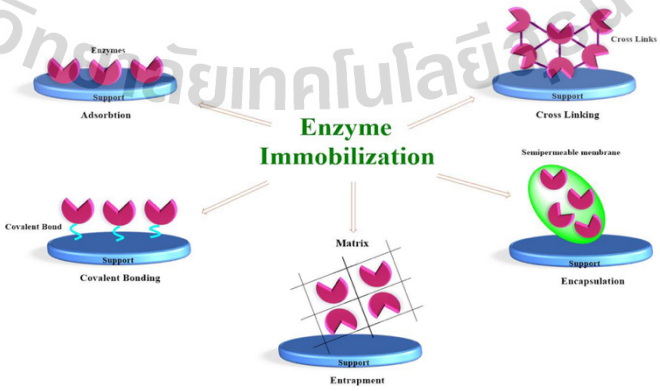

Figure 2.5 Different types of enzyme immobilization techniques.(Rana et al., 2022).

Adsorption involves the physical attachment of enzymes onto carriers through weak forces such as van der Waals interactions, hydrogen bonds, and ionic interactions. This method is simple and cost-effective, allowing easy recovery of the enzyme. However, the weak interactions can lead to enzyme leaching, affecting long-term stability (Rana et al., 2022).

Covalent binding forms strong covalent bonds between the enzyme and the support material, providing enhanced stability and reducing the risk of leaching. Despite its durability, covalent binding can alter the enzyme's active site, potentially reducing its activity (Rana et al., 2022).

Entrapment involves enclosing the enzyme within a matrix, such as a gel or polymer, allowing substrates and products to diffuse in and out while retaining the enzyme. This method maintains the enzyme's environment, preserving its activity. The main drawback is the potential mass transfer limitation, which can reduce the reaction rate (Rana et al., 2022).

Encapsulation is a technique where enzymes are confined within a semi-permeable membrane, protecting them from harsh conditions while allowing substrate and product movement. This method offers high stability and activity retention but can be complex and costly to implement on a large scale (Rana et al., 2022).

2.5 Bio-Electrochemistry

Bioelectrochemistry has emerged as a pivotal discipline at the interface of biology, chemistry, and electrochemical technology, offering sustainable solutions for energy conversion, biosensing, and environmental remediation (Chen et al., 2020). Central to this field is the harnessing of redox-active biomolecules—most notably enzymes and cofactors—that facilitate electron transfer processes between biological systems and electrodes. In microbial fuel cells and enzymatic biofuel cells, for

instance, understanding and optimizing these redox interactions is critical for improving current density, stability, and overall efficiency. Among the most critical determinants of bioelectrochemical function are the redox cofactors that shuttle electrons between biological molecules and electrodes. These cofactors, embedded within oxidoreductases, span a broad spectrum of midpoint redox potentials that enable directional electron flow in biological systems. According to the comprehensive ProtReDox database (Figure 2.6), the most reducing cofactors include the 4Fe–4S clusters (with an average redox potential of approximately –429 mV), followed by 2Fe–2S clusters (–309 mV) and flavins (around –186 mV), which include both FAD and FMN. More oxidizing cofactors, such as heme-bound iron centers, exhibit a wider range of potentials, typically averaging around +43 mV but extending as high as +197 mV depending on the specific heme environment. Even further toward the oxidizing end of the spectrum are molybdenum-based cofactors (+204 mV) and copper sites, which average +325 mV and can reach up to +530 mV in certain protein environments (McGuinness et al., 2024). These values are not intrinsic to the cofactors alone but are significantly modulated by the surrounding protein matrix through factors such as hydrogen bonding, solvation, electrostatics, and coordination geometry. Understanding these redox profiles is essential for matching engineered oxidoreductases with electrode materials and applied potentials in bioelectrochemical systems, ensuring efficient electron flow, energy conversion, and catalytic performance.

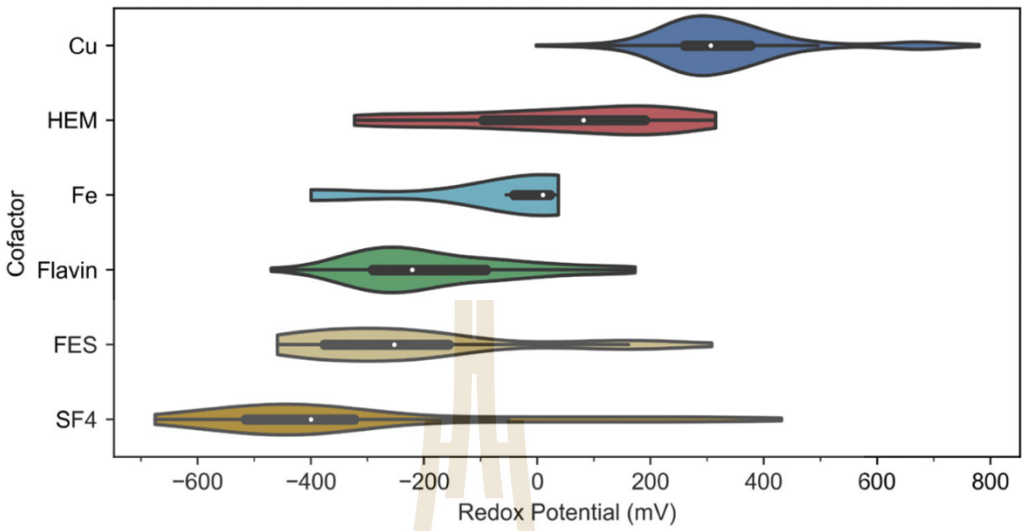

Figure 2.6 Distribution of redox potentials for the most abundant cofactor types. SF4 (4Fe4S; 82) 329 ± 268 mV; FES (2Fe2S; 64) 220 ± 199 mV; Flavin (114) 183 ± 141 mV; Fe (10) 72 ± 173 mV; HEM (42) 43 ± 190 mV; Cu (147) 333 ± 129 mV. The count of each cofactor type is within parentheses. (McGuinness et al., 2024).

Recent advancements in bioelectrochemical systems (BESs) have benefited immensely from protein engineering efforts that tailor redox enzymes to better interface with electrodes. Structural refinement of FAD-dependent glucose dehydrogenases (FAD-GDHs), for example, has improved their direct electron transfer capacity by optimizing active site geometry and introducing mutations that enhance surface binding or facilitate electron tunneling (Adachi et al., 2020). Similar strategies are being applied to cytochrome-based systems where domain engineering and fusion constructs enable more efficient electrical connectivity. The unique redox potential windows of these cofactors determine the compatibility of engineered enzymes with different electrode materials, influencing the thermodynamics and kinetics of the overall system.

Electrode material design is another cornerstone of bioelectrochemical innovation. Carbon nanostructures, doped graphene, and conductive polymers have

been increasingly adopted for their high surface area and redox compatibility. These materials are often chosen based on the redox potential of the enzyme-cofactor systems they support (Fredj et al., 2025).

In parallel, applications of BESs are expanding beyond energy generation into environmental detoxification and nutrient recovery. Bioelectrochemical processes now enable efficient ammonia and phosphate recovery from wastewater using redox reactions facilitated by microbial consortia and electrode-immobilized enzymes. These systems not only recover valuable nutrients but also reduce greenhouse gas emissions traditionally associated with chemical treatments. Importantly, the redox potential compatibility between microbial outer-membrane cytochromes and conductive supports directly governs the rate of such transformations (Kato et al., 2012).

From a broader perspective, the careful matching of enzyme-cofactor redox potential with electrode material properties and system design has emerged as a critical consideration for advancing bioelectrochemical devices. As such, bioelectrochemistry is evolving into a platform not only for sustainable energy solutions but also for uncovering fundamental redox biology principles at the materials interface. The continued integration of synthetic biology, structural bioinformatics, and electrochemical engineering is expected to unlock more efficient and durable systems that capitalize on nature's redox chemistry for a wide range of technological applications.

2.6 Biofuel cells

A biofuel cell (BFC) is an electrochemical device that harnesses biochemical reactions to generate electrical energy through the catalytic activity of biological materials, typically enzymes or microorganisms. Fundamentally, a BFC comprises two main compartments (Figure 2.1): the anode, where the bio-oxidation of a fuel occurs, and the cathode, where an oxidant is reduced. To complete the electrical circuit, these

half-cells are connected via an external circuit (allowing electron flow) and an internal ion-conducting path (like a proton exchange membrane or salt bridge). At the anode, a biological catalyst such as an oxidoreductase enzyme (e.g., glucose oxidase, glucose dehydrogenase, or other microbial enzymes) facilitates the oxidation of organic fuel molecules like glucose or lactate, releasing electrons and protons. These electrons travel through the external circuit, producing usable electrical power, while the protons diffuse through the membrane to reach the cathode side. At the cathode, another enzyme (commonly laccase or bilirubin oxidase) or microbial component catalyzes the reduction of molecular oxygen, typically to water. The reactions are as follows: at the anode, glucose can be oxidized to gluconolactone (in enzymatic systems) or further metabolized by microbes, producing CO_2, electrons, and protons. At the cathode, $O_2 + 4e^- + 4H^+ \longrightarrow 2H_2O$ is the typical terminal reaction. Importantly, the electrodes are often modified to enable either direct electron transfer (DET)—where electrons flow directly from the redox center of the biocatalyst to the electrode—or mediated electron transfer (MET), where artificial or naturally derived redox mediators shuttle electrons between the enzyme and the electrode surface. The success of a BFC depends critically on the immobilization of the biocatalyst, the conductivity and surface structure of the electrode, and the compatibility of the reaction conditions (e.g., pH, temperature) with the biological components. When combined with glucose-based or biomass-based systems, these fundamental reactions remain the foundation, with variations in the choice of fuel and biocatalyst, electron mediators, and electrode design tailored to the substrate's complexity. Thus, understanding this basic framework is essential for exploring advanced BFC architectures, such as those using breakdown and oxidase of cellobiose and complex plant-derived sugars by enzymes or microbial communities to convert biochemical energy into clean, sustainable electricity (Bartlett, 2008).

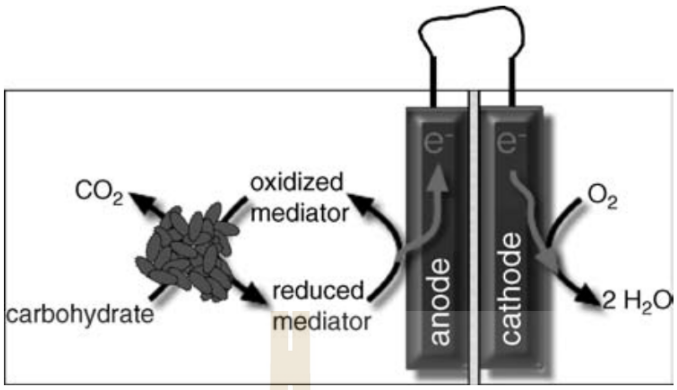

Figure 2.7 Configuration of a biofuel cell in which mediated electron transport between the microorganism and the anode occurs. Note that the microorganism and mediator may or may not be confined to the surface of the anode (Bartlett, 2008).

Glucose Fuel Cells:

Glucose fuel cells typically use glucose as the primary fuel source, converting it into electricity through enzymatic reactions. These cells often employ enzymes such as glucose oxidase or glucose dehydrogenase, which facilitate the oxidation of glucose, releasing electrons that generate an electrical current. For instance, a miniature glucose/O_2 biofuel cell with high tolerance against ascorbic acid (Figure 2.8) has been shown to provide significant power output, demonstrating the practical potential of glucose-based biofuel cells in various applications (Rafighi et al., 2022) .

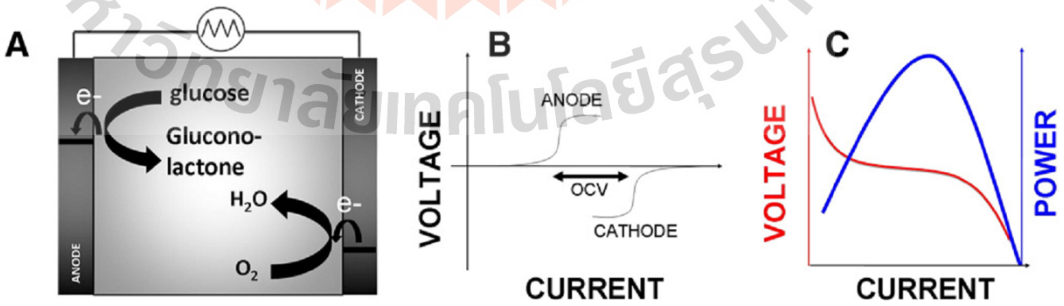

Figure 2.8 (A) Schematic representation of a glucose fuel cell (B) simulated polarization curve for bioanode and biocathode (C) schematic polarization curve and power profile of a fuel cells (Cosnier et al., 2014).

One significant advantage of glucose fuel cells is their compatibility with human physiological conditions, making them suitable for powering medical implants and other small devices. Studies have demonstrated the feasibility of operating glucose fuel cells *in vivo*, such as in rats, highlighting their potential for medical applications (Rafighi et al., 2022)

Biomass Fuel Cells:

Biomass fuel cells expand the range of biofuels to include complex carbohydrates and polysaccharides derived from plant and fungal cell walls. These cells utilize enzymes to hydrolyze polysaccharides into simpler sugars, which are then oxidized to produce electricity. Biomass-derived materials like cellulose and starch are particularly attractive due to their abundance and renewability (Rafighi et al., 2022).

Biomass fuel cells often employ a multi-enzyme cascade system to efficiently convert polysaccharides into monosaccharides or disaccharides, which are then oxidized. For instance, cellulose and starch have been used in multi-enzyme fuel cells to produce electrical energy, with starch-based cells utilizing a cascade of α-amylase, glucoamylase, and glucose oxidase enzymes (Rafighi et al., 2022). Similarly, disaccharides like sucrose have also been employed with invertase, generating multiple electrons per molecule and achieving high current densities (Rafighi et al., 2022).

Glucose and biomass fuel cells represent promising advancements in the field of renewable energy. By leveraging enzymatic biocatalysis to convert renewable biological materials into electrical energy, these fuel cells offer sustainable alternatives to conventional power sources. Their potential applications range from medical implants to portable electronic devices, showcasing the versatility and environmental benefits of biofuel cell technology.

2.7 Electron transfer mechanisms in enzyme-modified electrodes

Direct Electron Transfer (DET)

In the realm of enzymatic electrochemical systems, direct electron transfer (DET) (Figure 2.9a) represents one of the most elegant yet challenging mechanisms by which enzymes can communicate electrically with electrodes. This process occurs when electrons are transferred directly from the redox-active center of an enzyme—typically a tightly bound prosthetic group like FAD, heme, or copper centers—straight to the surface of an electrode, without the aid of any external mediators. This is a powerful concept because it removes the need for artificial electron shuttles, simplifying the system and improving both stability and specificity. However, achieving DET is far from straightforward. The active sites of enzymes are usually nestled deep within the folded protein structure, naturally designed to be shielded from random interactions in biological environments. This evolutionary design, while beneficial in nature, poses a significant barrier for electron tunneling in artificial settings. For DET to occur efficiently, electrons must traverse through the insulating amino acid matrix of the enzyme, and this tunneling becomes negligible beyond about 2 nanometers—a severe limitation (Flexer and Brun, 2017).

Mediated Electron Transfer (MET)

Mediated Electron Transfer (MET) (Figure 2.9b) plays a crucial role in enzymatic electrochemical systems, particularly when the enzyme's redox-active site is deeply embedded within its structure, making direct contact with the electrode surface difficult. In this mechanism, small, redox-active molecules known as mediators act as go-betweens: they shuttle electrons from the active site of the enzyme to the electrode. This is especially useful for oxidoreductases like glucose oxidase, whose flavin adenine dinucleotide (FAD) cofactor participates in redox reactions but is often inaccessible to the electrode. During MET, the enzyme catalyzes a reaction where it

either donates or accepts electrons via its cofactor, temporarily altering its redox state. The mediator then interacts with this cofactor—accepting or donating electrons as necessary—and subsequently undergoes its own redox reaction at the electrode surface, thereby regenerating its original state and enabling continuous electron flow. This cyclic process effectively bridges the biological and electrochemical components, enabling efficient energy conversion or sensing. Despite its advantages, MET systems must carefully balance factors such as mediator stability, reactivity, and potential toxicity, especially in biomedical applications. By optimizing mediator choice and enzyme immobilization strategies, MET provides a flexible and effective route for integrating biocatalysis with electrical signal transduction. (Xiao et al., 2019)

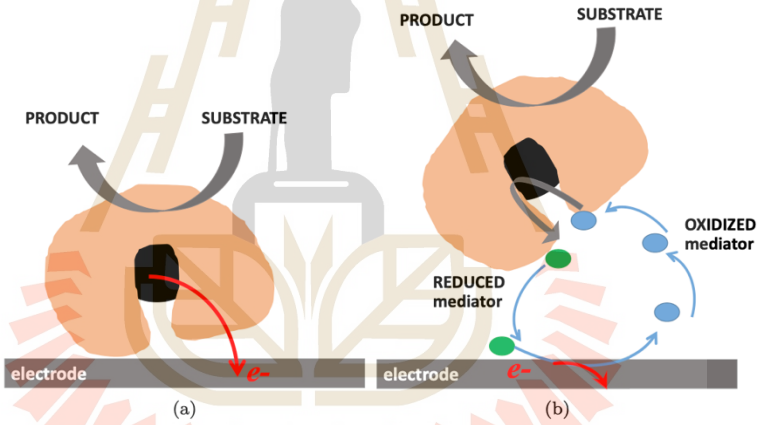

Figure 2.9 Schematic representation of electron transfer mechanisms between the enzyme and electrode. (a) Direct Electron Transfer (DET). (b) Mediated electron transfer (MET). (Flexer and Brun, 2017).

2.8 References

Adachi, T., Fujii, T., Honda, M., Kitazumi, Y., Shirai, O., and Kano, K. (2020). Direct electron transfer-type bioelectrocatalysis of FAD-dependent glucose dehydrogenase using porous gold electrodes and enzymatically implanted platinum nanoclusters. *Bioelectrochemistry*, *133*, 107457.

Algov, I., Feiertag, A., and Alfonta, L. (2021). Site-specifically wired and oriented glucose dehydrogenase fused to a minimal cytochrome with high glucose sensing sensitivity. *Biosensors & Bioelectronics*, *180*, 113117.

Badoni, V., Rana, G. S., Dubey, A., and Verma, A. K. (2025). β-Glucosidase production and its applications. In *Microbial Enzymes* (pp. 437–476). *John Wiley & Sons*, Ltd. Bartlett, P. N. (Ed.). (2008). *Bioelectrochemistry: Fundamentals, experimental techniques and applications*. *John Wiley & Sons.*

Cerutti, G., Gugole, E., Montemiglio, L. C., Turbé-Doan, A., Chena, D., Navarro, D., Lomascolo, A., Piumi, F., Exertier, C., Freda, I., Vallone, B., Record, E., Savino, C., and Sciara, G. (2021). Crystal structure and functional characterization of an oligosaccharide dehydrogenase from *Pycnoporus cinnabarinus* provides insights into fungal breakdown of lignocellulose. *Biotechnology for Biofuels*, *14*(1), 161.

Chatterjee, A., Puri, S., Sharma, P. K., Deepa, P. R., and Chowdhury, S. (2023). Nature-inspired Enzyme engineering and sustainable catalysis: Biochemical clues from the world of plants and extremophiles. *Frontiers in Bioengineering and Biotechnology*, *11*, 1229300.

Chen, H., Ma, L., Dai, H., Fu, Y., Wang, H., and Zhang, Y. (2022). Advances in Rational Protein Engineering toward Functional Architectures and Their Applications in Food Science. *Journal of Agricultural and Food Chemistry*, *70*(15), 4522–4533.

Chen, H., Simoska, O., Lim, K., Grattieri, M., Yuan, M., Dong, F., Lee, Y. S., Beaver, K., Weliwatte, S., Gaffney, E. M., and Minteer, S. D. (2020). Fundamentals, Applications, and Future Directions of Bioelectrocatalysis. *Chemical Reviews*, *120*(23), 12903–12993.

Cosnier, S., Le Goff, A., and Holzinger, M. (2014). Towards glucose biofuel cells implanted in human body for powering artificial organs: Review. *Electrochemistry Communications*, *38*, 19–23.

Flexer, V., and Brun, N. (2017). Fundamentals of Enzymatic Electrochemical Systems. In N. Brun & V. Flexer, *Functional Electrodes for Enzymatic and Microbial Electrochemical Systems* (pp. 3–50). WORLD SCIENTIFIC (EUROPE).

Fredj, Z., Rong, G., and Sawan, M. (2025). Recent Advances in Enzymatic Biofuel Cells to Power Up Wearable and Implantable Biosensors. *Biosensors*, *15*(4), Article 4.

Gao, P., Peng, S., Sam, F. E., Zhu, Y., Liang, L., Li, M., and Wang, J. (2022). Indigenous Non-Saccharomyces Yeasts With β-Glucosidase Activity in Sequential Fermentation With Saccharomyces cerevisiae: A Strategy to Improve the Volatile Composition and Sensory Characteristics of Wines. *Frontiers in Microbiology*, *13*.

Grigorakis, K., Ferousi, C., and Topakas, E. (2025). Protein Engineering for Industrial Biocatalysis: Principles, Approaches, and Lessons from Engineered PETases. *Catalysts*, *15*(2), Article 2.

Hua, L., Qianqian, B., Jianfeng, Z., Yinbiao, X., Shengyu, Y., Weishi, X., Yang, S., and Yupeng, L. (2022). Directed evolution engineering to improve activity of glucose dehydrogenase by increasing pocket hydrophobicity. *Frontiers in Microbiology*, *13*, 1044226.

Ito, K., Okuda-Shimazaki, J., Kojima, K., Mori, K., Tsugawa, W., Asano, R., Ikebukuro, K., and Sode, K. (2021). Strategic design and improvement of the internal electron transfer of heme b domain-fused glucose dehydrogenase for use in direct electron transfer-type glucose sensors. Biosensors & Bioelectronics, *176*, 112911.

Kato, S., Hashimoto, K., and Watanabe, K. (2012). Microbial interspecies electron transfer via electric currents through conductive minerals. *Proceedings of the National Academy of Sciences*, *109*(25), 10042–10046.

Ketudat Cairns, J. R., and Esen, A. (2010). β-Glucosidases. *Cellular and Molecular Life Sciences, 67*(20), 3389–3405.

Komori, H., Inaka, K., Furubayashi, N., Honda, M., and Higuchi, Y. (2015). Crystallographic analysis of FAD-dependent glucose dehydrogenase. *Acta Crystallographica. Section F, Structural Biology Communications*, *71*(Pt 8), 1017–1019.

Maicas, S., and Mateo, J. J. (2016). Microbial Glycosidases for Wine Production. *Beverages*, *2*(3), Article 3.

McGuinness, K. N., Fehon, N., Feehan, R., Miller, M., Mutter, A. C., Rybak, L. A., Nam, J., AbuSalim, J. E., Atkinson, J. T., Heidari, H., Losada, N., Kim, J. D., Koder, R. L., Lu, Y., Silberg, J. J., Slusky, J. S. G., Falkowski, P. G., and Nanda, V. (2024). The energetics and evolution of oxidoreductases in deep time. *Proteins: Structure, Function, and Bioinformatics*, *92*(1), 52–59.

Neubacher, S., Saya, J. M., Amore, A., and Grossmann, T. N. (2020). In Situ Cyclization of Proteins (INCYPRO): Cross-Link Derivatization Modulates Protein Stability. *The Journal of Organic Chemistry*, *85*(3), 1476–1483.

Okuda-Shimazaki, J., Yoshida, H., and Sode, K. (2020). FAD dependent glucose dehydrogenases—Discovery and engineering of representative glucose sensing enzymes. *Bioelectrochemistry (Amsterdam, Netherlands)*, *132*, 107414.

Pan, X., and Kortemme, T. (2021). Recent advances in *de novo* protein design: Principles, methods, and applications. *Journal of Biological Chemistry*, *296*, 100558.

Qiu, Y., and Wei, G.-W. (2023). Artificial intelligence-aided protein engineering: From topological data analysis to deep protein language models.

Rafighi, P., Nordberg Karlsson, E., Zubaida Gulshan Ara, K., Pankratova, G., Bollella, P., Peterbauer, C. K., and Gorton, L. (2022). A novel membraneless β-glucan/O2 enzymatic fuel cell based on β-glucosidase (RmBgl3B)/pyranose dehydrogenase (AmPDH) co-immobilized onto buckypaper electrode. *Bioelectrochemistry*, *148*, 108254.

Rana, H., Sharma, A., Dutta, S., and Goswami, S. (2022). Recent Approaches on the Application of Agro Waste Derived Biocomposites as Green Support Matrix for Enzyme Immobilization. *Journal of Polymers and the Environment*, *30*(12), 4936–4960.

Romo-Sánchez, S., Arévalo-Villena, M., García Romero, E., Ramirez, H. L., and Briones Pérez, A. (2014). Immobilization of β-Glucosidase and Its Application for Enhancement of Aroma Precursors in Muscat Wine. *Food and Bioprocess Technology*, *7*(5), 1381–1392.

Singh, G., Verma, A. K., and Kumar, V. (2016). Catalytic properties, functional attributes and industrial applications of β-glucosidases. *3 Biotech*, *6*(1), 3.

Tran, T. N. A., Son, J.-S., Awais, M., Ko, J.-H., Yang, D. C., & Jung, S.-K. (2023). β-Glucosidase and Its Application in Bioconversion of Ginsenosides in Panax ginseng. *Bioengineering*, *10*(4), Article 4.

Wang, Y., Zhang, J., Han, B., Tan, L., Cai, W., Li, Y., Su, Y., Yu, Y., Wang, X., Duan, X., Wang, H., Shi, X., Wang, J., Yang, X., and Liu, T. (2023). Noncanonical amino acids as doubly bio-orthogonal handles for one-pot preparation of protein multiconjugates. *Nature Communications*, *14*(1), 974.

Xiao, X., Xia, H., Wu, R., Bai, L., Yan, L., Magner, E., Cosnier, S., Lojou, E., Zhu, Z., and Liu, A. (2019). Tackling the Challenges of Enzymatic (Bio)Fuel Cells. *Chemical Reviews*, *119*(16), 9509–9558.

Xu, S.-Y., Zhou, L., Xu, Y., Hong, H.-Y., Dai, C., Wang, Y.-J., and Zheng, Y.-G. (2023a). Recent advances in structure-based enzyme engineering for functional reconstruction. *Biotechnology and Bioengineering*, *120*(12), 3427–3445.

Xu, S.-Y., Zhou, L., Xu, Y., Hong, H.-Y., Dai, C., Wang, Y.-J., and Zheng, Y.-G. (2023b). Recent advances in structure-based enzyme engineering for functional reconstruction. *Biotechnology and Bioengineering*, *120*(12), 3427–3445.

Yang, K. K., Wu, Z., and Arnold, F. H. (2019). Machine-learning-guided directed evolution for protein engineering. *Nature Methods*, *16*(8), 687–694.

Zhang, P., Zhang, R., Sirisena, S., Gan, R., and Fang, Z. (2021). Beta-glucosidase activity of wine yeasts and its impacts on wine volatiles and phenolics: A mini-review. *Food Microbiology*, *100*, 103859.

CHAPTER III

MATERIALS AND METHODS

3.1 Chemical, Plasmid, and Strain

Laboratory materials and preparation were conducted in the laboratories of Prof. Dr. James Ketudat-Cairns and Asst. Prof. Dr. Piyanut Pinyou, as well as at the Center of Scientific and Technological Equipment, Suranaree University of Technology. All chemicals were purchased from either Sigma-Aldrich or Tokyo Chemical Industry (TCI). Oligonucleotides were obtained from Bio Basic Inc. The wild-type *At*BGL5 gene, encoding *Agrobacterium tumefaciens* β-glucosidase 5 and optimized for expression in *Escherichia coli*, was synthesized by Twist Bioscience and cloned into the pET30a expression vector by Chamaipon Beagbandee to yield pET30a/AtBGL5. A codon-optimized gene for *Talaromyces emersonii* FAD-dependent glucose dehydrogenase (*Te*-GlcDH) expression in *E. coli* was synthesized by Gene Universal and cloned into the *Nco*I and *Xba*I sites of the pET32a vector (referred to as pET32-GlcDH in this study).

For site-directed mutagenesis, mutant plasmids encoding β-glucosidase variants C174V and H229S were constructed by the QuikChange site-directed mutagenesis method (Agilent Technologies). This method involves the use of complementary oligonucleotide primers containing the desired mutation to thermally amplify the entire plasmid DNA. After amplification, the reaction mixture was treated with the restriction enzyme DpnI to digest the original (methylated) template plasmid, leaving only the newly synthesized (mutated) DNA. The mutated plasmids were then transformed into chemically competent *E. coli* cells for propagation and sequence-

verification. **Tables 3.1**, **3.2**, and **3.3** list the bacterial strains, oligonucleotides, and plasmids used, respectively.

Table 3.1 List of strains used in this study.

Strain	Description	Reference
Escherichia coli BL21(DE3)	Host for protein expression	JKC Lab
E. coli XL1-blue	Strain for propagating plasmid	JKC Lab

Table 3.2 List of oligonucleotides used in this study. “f” and “r" stand for the forward primer and reverse primer, respectively.

Primers	Sequence 5’ to 3’	Description
AgBGlu_H229S-f	CTCGTTCTCAATGCATCCAGCGTGATCCCCGCCTC	Primer for site-directed mutagenesis (H229S) for beta-glucosidase 5 from *Agrobacterium tumefaciens* GH1 family
AgBGlu_H229S-r	GAGGCGGGGATCACGCTGGATGCATTGAGAACGAG	
AgBGlu_C179V-f	GACGTTTAATGAACCTTGGGTGGCCGTCTGGCTGTCC	Primer for site-directed mutagenesis (C174V) for beta-glucosidase 5 from *Agrobacterium tumefaciens* GH1 family
AgBGlu_C179V-r	GGACAGCCAGACGGCCACCCAAGGTTCATTAAACGTC	

Table 3.3 List of plasmids used in this study.

Strain	Description	Reference
pET30a	Plasmid for protein expression	Novagen (Merck)
pET30a/AtBGL5	Plasmid for protein expression of AtBGL5	JKC Lab
pET32a	Plasmid for protein expression	Novagen (Merch)
pET32a/GlcDH	Plasmid for expression of FAD-dependent glucose dehydrogenase	JKC Lab
pET30a/AtBGL5-H229S	Plasmid for expression of AtBGLU H229S	JKC Lab
pET30a/AtBGL5-C174V	Plasmid for expression of AtBGLU C174V	JKC Lab

3.2 Protein Expression and Overexpression

The cells of *E. coli* strain BL21(DE3) containing the plasmid pET30a-AtBGL or pET32a-TeGlcDH were grown in 20 mL of Luria-Bertani (LB) medium supplemented with either 50 µg/mL ampicillin for cells carrying pET32a/TeGDH or kanamycin at a final concentration of 15 µg/mL for cells containing pET30a-derived vectors and incubated at 37 °C overnight. Ten milliliters of the overnight culture were then inoculated into 1 L of fresh LB medium containing the same antibiotic concentrations. The culture was shaken at 200 rpm and 37 °C until it reached an OD_{600} of approximately 0.6–0.7. Isopropyl-β-D-1-thiogalactopyranoside (IPTG) was added to a final concentration of 200 µM to induce protein overexpression. The culture was subsequently incubated at 20 °C

with shaking overnight. Cells were harvested by centrifugation at 5,000 rpm for 25 minutes at 8 °C to collect the cell pellet.

3.3 Purification of AtBGL and TeGlcDH

The cell pellet was resuspended in 20 mL of lysis buffer. The cells were lysed and incubated at room temperature for 30 minutes, followed by centrifugation at 12,879 xg and 4 °C for 20 minutes. The resulting supernatant (cell lysate) was applied to an IMAC column that had been pre-equilibrated sequentially with 150 mM NaCl in 20 mM phosphate buffer (pH 7.5) (equilibration buffer), H_2O, 100 mM $CoCl_2$, H_2O, 500 mM NaCl, H_2O, and equilibration buffer. The nonspecific proteins were washed off and the bound protein was eluted stepwise with equilibration buffer containing 5 mM, 10 mM, 250 mM, and 500 mM imidazole. After elution, TeGlcDH was incubated with 100 µL of 1 mM FAD to ensure cofactor incorporation. Both TeGlcDH and AtBGL5 proteins were then concentrated and buffer-exchanged into 20 mM Tris-HCl (pH 7.5), 150 mM NaCl in a Centricon® centrifugal filter device with a 30,000 MWCO (Millipore). The protein concentrations were determined by measuring absorbance at 280 nm on a Nanodrop UV-Vis spectrophotometer. A volume of 2 µL of each protein sample was applied to the pedestal, and the absorbance was recorded after blanking the instrument with the same buffer used for sample preparation. The protein concentrations were calculated by the Beer-Lambert Law, with specific extinction coefficients applied: 1.806 Abs for 0.1% = 1 g/L for AtBGL and 1.479 Abs for 0.1% = 1 g/L for TeGlcDH, which assume that all cysteine residues were in the reduced form Expasy (*Expasy - ProtParam*, n.d.). After quantification, the purified proteins were aliquoted and stored at –20 °C.

3.4 Enzymatic assay

β-glucosidase activity was measured by monitoring the release of *p*-nitrophenol (pNP) from *p*-nitrophenyl-β-D-glucopyranoside (pNPGlc) based on its absorbance at 405 nm measured in a Thermo Scientific™ Multiskan™ GO microplate spectrophotometer. The β-glucosidase assay reactions were carried out in a total volume of 140 µL, containing 0.1, 0.5, or 1 mM pNPGlc and 0.01 µg/µL AtBGL5 in 50 mM phosphate buffer (pH 6.0). The reactions were incubated for 15 minutes and then stopped by the addition of 2 M Na_2CO_3. Control reactions that did not contain AtBGL5 served as blanks to correct for background absorbance.

In addition to the *p*NP-based assay, the amount of reducing sugars released during biomass digestion was quantified using the 3,5-dinitrosalicylic acid (DNS) assay. Biomass digestion reactions were conducted using 100 mg of sugarcane leaf powder as the substrate and 2% (w/w) glycoside hydrolases (GH) in 50 mM citrate-phosphate buffer (pH 5.5) in 10 mL total volume. The reactions were incubated overnight at optimal conditions to allow enzymatic hydrolysis. To terminate the reactions, 200 µL aliquots were removed and immediately boiled for 5 minutes. 50 µL DNS reagent was then added to each aliquot, followed by an additional 5-minute boiling step to enable color development through the reduction of DNS by the released reducing sugars. After cooling the samples to room temperature, absorbance was measured at 540 nm in a spectrophotometer. The concentration of reducing sugars was quantified by comparison to a standard curve prepared with known concentrations of glucose.

For TeGlcDH, enzyme activity assays were performed in a total volume of 200 µL, containing 140 µM 1-methoxy-5-methylphenazinium methyl sulfate (1-mPMS), 70 µM 2,6-dichlorophenol indophenol (DCPIP), 0.2% Triton X-100, 300 mM glucose, and 0.1 µg of TeGlcDH in 20 mM sodium phosphate buffer with 150 mM NaCl (pH 7.5). Control reactions were prepared under identical conditions but without the enzyme to account

for non-enzymatic reduction of DCPIP. Reaction progress was monitored by measuring the decrease in absorbance at 600 nm, corresponding to the reduction of DCPIP, in a microtiter plate reader spectrophotometer in a continuous assay format. Absorbance readings were recorded every 10 seconds over a 15-minute period. To determine kinetic parameters, initial reaction velocities were measured at varying concentrations of glucose (50 – 2000 mM) while maintaining all other components constant. The initial rates were derived from the linear portion of the absorbance vs. time curves. These rates were then plotted against substrate concentrations to generate a Michaelis-Menten curve. Nonlinear regression analysis in GraFit5 software was performed to fit the data to the Michaelis-Menten equation, allowing the calculation of kinetic parameters including the Michaelis constant (K_m) and maximum reaction velocity (V_{max}). These apparent parameters provide insights into the substrate affinity and catalytic efficiency of TeGlcDH under the specified assay conditions.

3.5 Bioelectrode Preparation and Electrochemical Characterization

After determining the kinetic parameters (K_m, V_{max}, $k_{cat,}$ and k_{cat}/K_m) of *At*BGL5 and *Te*GlcDH, both enzymes were tested in a cascade reaction for biomass degradation and current generation via mediated electron transfer (MET). For the bioanode, a screen-printed carbon electrode (model MTE-300-G) was purchased from Zensor (Taichung City, Taiwan). The electrode consisted of a 3 mm diameter graphene working electrode (WE), a graphene counter electrode (CE), and a silver pseudoreference electrode (RE). TeGlcDH (40 µg) was immobilized by physisorption, followed by overnight crosslinking with 80 µg polyethyleneimine-ferrocene (PEI-Fc) and 21 µg poly(ethylene glycol) diglycidyl ether (PEGDE). To prepare the biocathode, 20 µL of 4 mg/mL 1-pyrenebutyric acid N-hydroxysuccinimide ester (PBSE) in dimethylformamide (DMF) was drop-cast onto a 9 mm graphene-coated polyimide

electrode. After a 30-minute room-temperature incubation to enable π-π stacking with the graphene surface, the electrode was rinsed with DMF to remove unbound PBSE and air-dried. Next, 100 µg of horseradish peroxidase (HRP) for 20 µL was applied and dried at room temperature. Finally, 2 µL of 5% (w/v) Nafion solution was added to immobilize and protect the enzyme layer. The completed biocathode was stored at 4°C overnight for stabilization. Once the electrodes were assembled, electrochemical measurements including cyclic voltammetry (CV), chronoamperometry, electrochemical impedance spectroscopy (EIS), and open circuit potential (OCP) were conducted. A Palmsens 4 potentiostat/galvanostat (Palmsens, the Netherlands) was employed to carry out the electrochemical measurements throughout this study.

3.6 Biofuel Cell Measurement

To evaluate the performance of the biofuel cell, a two-compartment electrochemical setup was meticulously assembled, with the compartments separated by a Nafion™ 117 proton exchange membrane to allow selective ion transport while preventing direct mixing of the anodic and cathodic solutions. The bioanode, consisting of glucose dehydrogenase (TeGlcDH) immobilized on a screen-printed graphene working electrode, was connected to the working terminal of the potentiostat. It was immersed in the anodic compartment containing 20 mL of 100 mM sodium phosphate buffer (pH 7.0) with 150 mM NaCl. To initiate the cascade reaction, 100 mM cellobiose and 1 mg of AtBGL5 β-glucosidase were added, enabling enzymatic hydrolysis of cellobiose into glucose, the substrate for TeGlcDH. Simultaneously, the biocathode, comprising horseradish peroxidase (HRP), was connected to the combined counter and reference terminals and immersed in the cathodic compartment containing 25 mL of electrolyte solution composed of 10 mM hydrogen peroxide (H_2O_2) and 1 mM AzBTS (azino-bis (3-ethylbenzothiazoline-6-sulfonic acid)), which served as an electron

mediator. The distance between the bioanode and biocathode was maintained at 8 cm. The temperature of both compartments was controlled and kept constant at 37°C throughout the experiment. After the addition of AtBGL5, the anolyte was incubated for 15 minutes to allow sufficient glucose production and stabilization of enzymatic activity. Once equilibrium was reached, the open-circuit voltage (OCV) of the biofuel cell was measured. Subsequently, multiple-potential chronoamperometry was performed in a sequence of potential steps ranging from 0.010 V to 0.650 V relative to the OCV. The current response at each step was recorded, and the resulting data were used to construct polarization and power curves, providing detailed insight into the electron transfer behavior and energy-conversion efficiency of the enzymatic biofuel cell system.

3.7 Reference

Expasy—ProtParam. (n.d.). Retrieved Jan 11, 2025, from web.expasy.org/protparam/

CHAPTER IV
RESULTS AND DISCUSSION

4.1 Preparation of Enzymes

The AtBGL5 beta-glucosidase and its H229S mutant, which was previously described to be more glucose tolerant (Goswami et al., 2021), were expressed in *E. coli* and purified by immobilized metal affinity chromatography (IMAC) to give proteins that were about 80-90% pure, based on SDS-PAGE (Figure 4.1a and b). Similarly, the TeGlcDH, which has been described as an efficient glucose dehydrogenase (Okuda-Shimazaki et al., 2020) was expressed in *E. coli* as a 79 kDa thioredoxin-glucose dehydrogenase fusion protein and purified by IMAC to give a major band of the expected size with similar purity

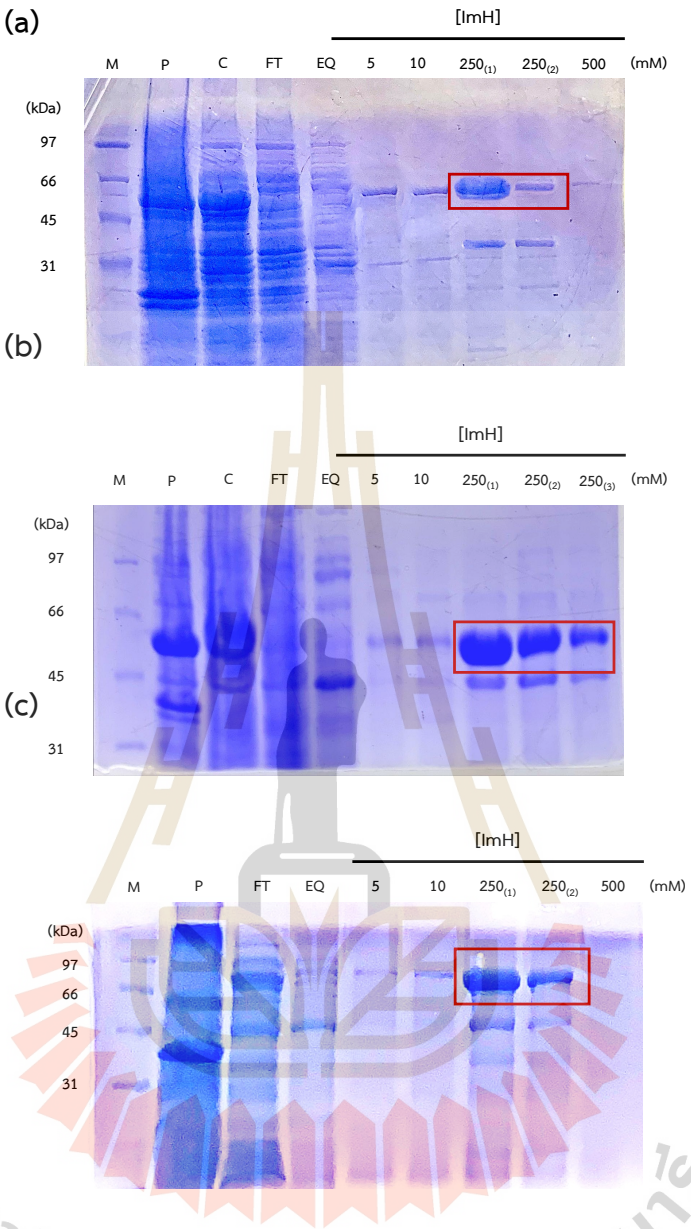

Figure 4.1 SDS-PAGE analysis showing results for (a) AtBGL5 and (b) AtBGL5-H229S, with approximate molecular weights of 57.7 kDa and 57.8 kDa, respectively, and (c) TeGlcDH, with an approximate molecular weight of 79 kDa.The labels M, P, C, FT, EQ, and ImH represent Marker, Pellet, Crude extract, Flow-through, Equilibration buffer wash, and washes and elution with different concentrations of Imidazole, respectively.

4.2 Kinetic characterization of AtBGL5, AtBGL5-H229S and TeGlcDH

β-Glucosidase kinetics for AtBGL5 and AtBGL5-H229S

A time-course experiment using the p-nitrophenyl-β-D-glucopyranoside (*p*NPGlc) assay was conducted to determine the initial reaction rate and optimal incubation time for the *Agrobacterium tumefaciens* β-glucosidase AtBGL5 and its mutant AtBGL5-H229S (Goswami et al., 2021). We found that the optimal enzyme concentration for both variants was 0.01 µg, with an incubation time of 15 minutes. These conditions were essential for ensuring accurate and reproducible measurements in subsequent kinetic analyses. The selection of an appropriate incubation time is critical in enzymatic assays. If the reaction is too short, there may not be enough product formation (*p*-nitrophenol in this case) to measure reliably, leading to underestimated activity. Conversely, if the incubation is too long, substrate depletion or product accumulation could introduce nonlinearity, affecting the accuracy of initial rate calculations. Similarly, enzyme concentration must be carefully optimized too much enzyme can cause the reaction to complete rapidly, making it difficult to capture the linear phase, while too little enzyme may result in weak or undetectable signals. By optimizing both parameters, we ensured that the enzymatic reaction stayed within the linear range, allowing for precise determination of kinetic constants.

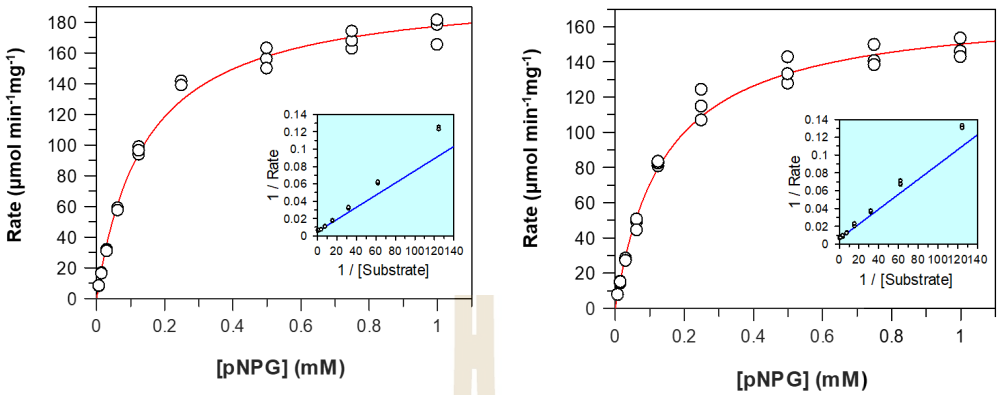

Figure 4.2 The Michaelis-Menten curves of AtBGL5 and AtBGL5-H229S hydrolysis of *p*NPGlc. The initial rate of reaction against the concentration of *para*-nitrophenyl-β-D-glucopyranoside (*p*NPG).

Table 4.1 The table of the kinetic parameters of AtBGL5 and AtBGL5-H229S hydrolysis of *p*NPGlc

Kinetic parameter	K_m (mM)	V_{max} (µmol $min^{-1}mg^{-1}$)	k_{cat} (s^{-1})	k_{cat}/K_m ($s^{-1}mM^{-1}$)
*At*BGL5	0.14 ± 0.01	202.5 ± 3.9	194.9 ± 3.7	1390
*At*BGL5-H229S	0.14 ± 0.01	171.6 ± 3.3	165.0 ± 3.1	1180

The kinetic analysis of the AtBGL5 and AtBGL5-H229S (mutant) enzymes hydrolysis of *p*NPGlc revealed that both exhibited similar K_m values, indicating that the mutation did not significantly alter the substrate concentration dependence. However, the mutant enzyme showed an approximate 20% reduction in V_{max}, k_{cat}, and k_{cat}/K_m compared to the wild type. This suggests that while the catalytic turnover and overall catalytic efficiency of the mutant are slightly compromised, the substrate interaction at the active site remains largely unchanged.

FAD-dependent Glucose dehydrogenase, TeGlcDH

Building upon the kinetic investigation of β-glucosidase, it is essential to characterize the kinetic behavior of FAD-dependent glucose dehydrogenase (FAD-GDH) from *Talaromyces emersonii* to support its integration into biomass conversion and bioelectrochemical systems. In this study, a continuous spectrophotometric assay was employed to monitor enzyme activity via the reduction of 2,6-dichlorophenolindophenol (DCPIP), coupled with the electron mediator 1-methoxyphenazine methosulfate (1-mPMS). Absorbance changes at 600 nm (A_{600}) were recorded at 10-second intervals, allowing for real-time tracking of the enzymatic oxidation of glucose. The initial velocity of the reaction was determined across varying glucose concentrations, enabling the derivation of Michaelis-Menten kinetic parameters. Optimal conditions were established using 0.1 µg of TeGlcDH, with incubation sustained for approximately 15 minutes, or until the reaction plateaued, indicating substrate depletion or equilibrium. This approach provides a reliable measure of enzyme performance under steady-state conditions and is crucial for evaluating its potential in redox-driven applications, including biofuel cells. Precise kinetic profiling under these assay conditions facilitates a deeper understanding of TeGlcDH catalysis and informs the rational design of multi-enzyme systems for sustainable energy and bioconversion technologies.

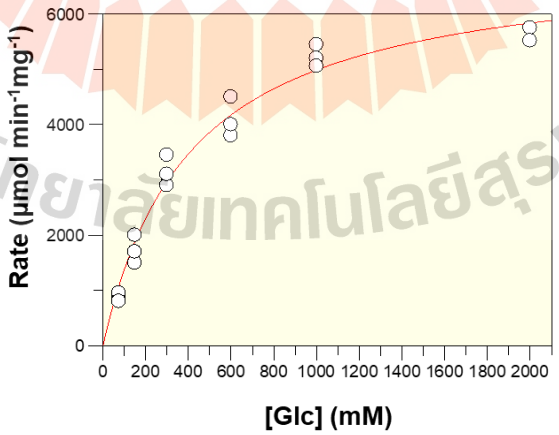

Figure 4.3 The Michaelis-Menten curves of TeGlcDH oxidation of glucose (Glc). The initial rate of reaction against the concentration of Glc is measured by the consumption of 2,6-dichlorophenolindophenol (DCPIP).

Table 4.2 The table of the kinetic parameters of FAD-GlcDH.

Kinetic parameter	K_m (mM)	V_{max} (μmol $min^{-1}mg^{-1}$)	k_{cat} (s^{-1})	k_{cat}/K_m ($s^{-1}mM^{-1}$)
FAD-GlcDH	411 ± 42	7040 ± 260	9270 ± 340	22.5

The kinetic parameters of *T. emersonii* FAD-dependent glucose dehydrogenase (TeGlcDH) for glucose, characterized by a high K_m value of 411 ± 42 mM, a V_{max} of 7040 ± 260 μmol·min^{-1}·mg^{-1}, a k_{cat} of 9270 ± 340 s^{-1}, and a catalytic efficiency k_{cat}/K_m of 22.5 s^{-1}·mM^{-1}, suggest an enzyme with exceptionally high catalytic turnover. The elevated K_m indicates that TeGlcDH requires a high concentration of glucose to achieve half-maximal velocity, which may favor high-throughput catalysis under conditions where glucose is abundant, such as in industrial or physiological environments where substrate concentration is not limited. The remarkably high k_{cat} implies that once glucose is bound, the enzyme rapidly completes the catalytic cycle, consistent with the behavior of oxidoreductases designed for fast redox turnover. However, the moderate catalytic efficiency k_{cat}/K_m indicates that while the enzyme is fast, it is not particularly efficient at low glucose concentrations, which could impact its performance in biosensing or diagnostic applications requiring sensitivity at lower substrate levels. This kinetic profile suggests that TeGlcDH is evolutionarily or biotechnologically optimized for high-output glucose oxidation rather than substrate economy, making it suitable for applications like biofuel cells or industrial glucose monitoring, where high substrate concentrations and robust electron transfer are essential.

4.3 Glucose and 1,5-δ-Gluconolactone Inhibition of AtBGL5 and AtBGL5-H229S

Glucose inhibition

β-Glucosidases play a crucial role in the final step of cellulose degradation by converting β-glucosides into glucose. However, a major limitation in their application, especially in biomass conversion processes, is product inhibition by glucose. Many β-glucosidases experience reduced activity at high glucose concentrations, which can hinder overall efficiency. This is true for AtBGL5 from *Agrobacterium tumefaciens*, which is known to be inhibited by its product, although to a lesser degree than some enzymes (Goswami et al., 2021). To address this, a mutant variant, AtBGL5-H229S, was engineered to enhance glucose tolerance (Goswami et al., 2021).

Following the successful determination of kinetic parameters for both AtBGL5 and its mutant, we proceeded to investigate the extent of glucose inhibition and to quantify the inhibition constants (K_i). Understanding the inhibitory effect of glucose is essential for evaluating the practical utility of the mutant enzyme under industrial conditions where glucose accumulation may occur.

AtBGL5

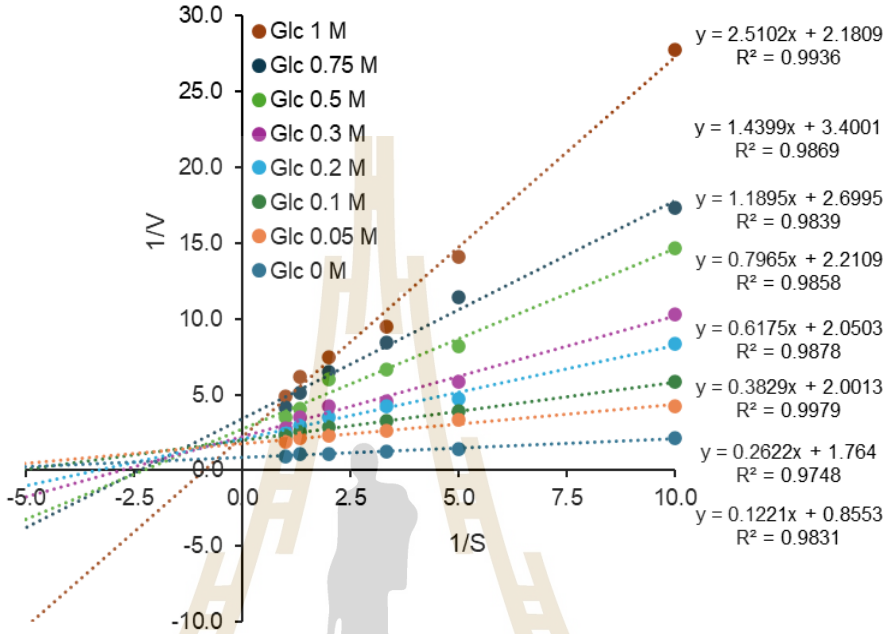

Figure 4.4 The Lineweaver-Burk plots of AtBGL5 in the presence of different concentrations of glucose. The inverse of the initial rate (1/v0) is plotted against the inverse of the *p*NPGlc substrate concentration (1/[substrate] at different inhibitor concentrations

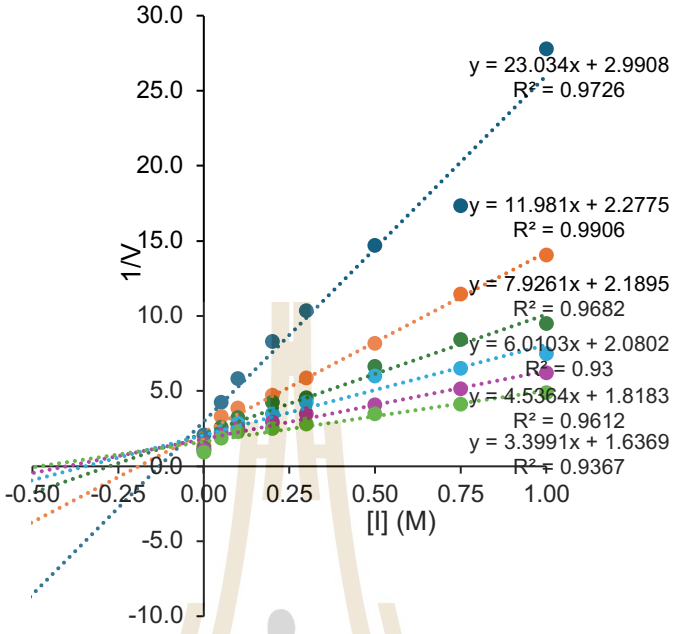

Figure 4.5 The Dixon plot of AtBGL5 inhibition by glucose. The inverse of the initial rate ($1/v_0$) is plotted against the concentration of inhibitor (glucose) at different substrate concentrations.

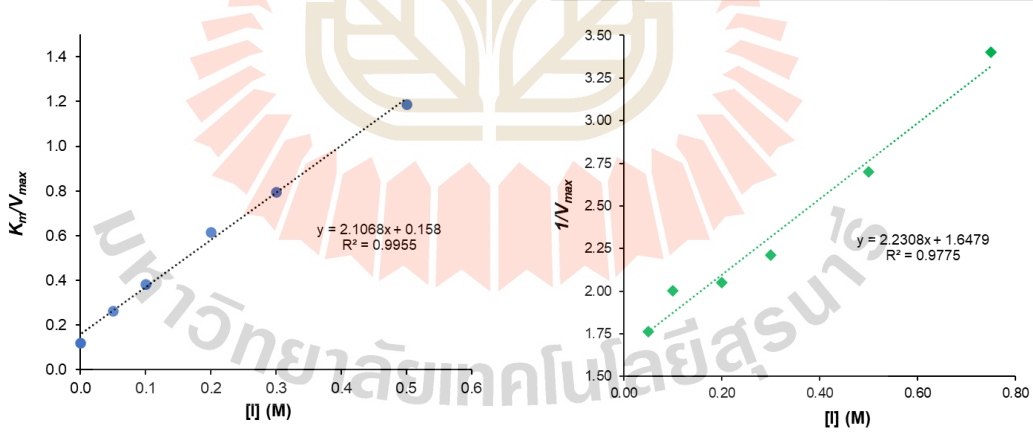

Figure 4.6 The derivative plots of AtBGL5 inhibition by glucose. (a) The Michaelis-Menten constant (K_m) divided by the maximum velocity (V_{max}) against the concentration of inhibitor (glucose). and (b) the inverse of the maximum velocity ($1/V_{max}$) is plotted against the concentration of inhibitor (glucose).

Table 4.3 The inhibition constants for AtBGL obtained from the derivative plots. The competitive inhibition constant (K_{ic}) is derived from Figure 4.6.a and the uncompetitive inhibition constant (K_{iu}) from Figure 4.6.b.

Inhibition constant	Value (mM)
competitive (K_{ic})	75 ± 11
uncompetitive (K_{iu})	674 ± 64

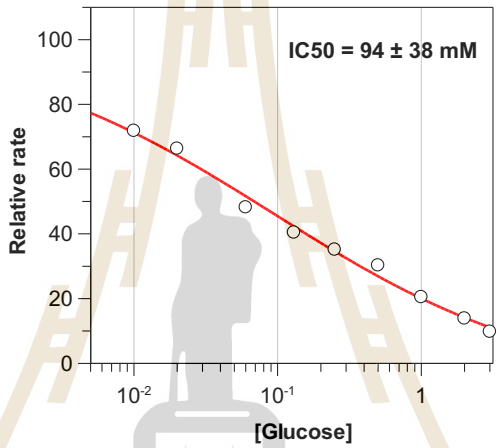

Figure 4.7 The 50% inhibitory concentration (IC50) of Glucose for the AtBGL5. The assay was performed at a fixed pNPGlc concentration of 1 mM, with glucose concentrations ranging up to 3 M.

The glucose inhibition profile we determined for wild-type *Agrobacterium tumefaciens* ß-glucosidase 5 (AtBGL5) reveals a substantially stronger inhibitory effect than previously reported by (Goswami et al., 2021). Our kinetic analysis showed a mixed-type inhibition mechanism (Figure 4.4), with a competitive inhibition constant (K_{ic}) of 75 ± 11 mM and an uncompetitive constant (K_{iu}) of 674 ± 64 mM. Additionally, the IC_{50} was measured at 94 ± 38 mM (Figure 4.7). These values sharply contrast with the K_i of 686 mM reported by (Goswami et al., 2021) for the same wild-type enzyme. Such a large discrepancy suggests either a fundamental difference in experimental conditions or a possible overestimation in the earlier study. While the previous work presented a single apparent K_i, my approach provides a more detailed breakdown of

inhibition kinetics, distinguishing between binding to the free enzyme and the enzyme-substrate complex. The low K_{ic} and IC_{50} values indicate that glucose inhibits AtBGL5 far more effectively than previously acknowledged, especially at concentrations relevant to industrial biomass hydrolysis. These results challenge the earlier characterization of the wild type as "moderately glucose-tolerant" and underscore the enzyme's vulnerability to product inhibition under glucose-rich conditions. This finding reinforces the need for precise kinetic profiling in enzyme characterization and highlights the critical importance of improving glucose tolerance through targeted mutagenesis, such as the H229S variant previously reported (Goswami et al., 2021).

AtBGL5-H229S

The H229S mutation originates from prior engineering efforts aimed at improving the glucose tolerance of β-glucosidase from *Agrobacterium tumefaciens* 5A (Goswami et al., 2021). In the native enzyme, glucose acts as a product inhibitor, posing a challenge for sustained enzymatic activity during high-load biomass saccharification. To address this, histidine at position 229, located near the entrance of the active site, was substituted with serine, a smaller and less polar residue. This substitution was hypothesized to reduce inhibitory interactions with glucose by modifying the local environment of the active site, potentially altering substrate accessibility or product release. Previous studies reported that this single-point mutation led to a notable increase in glucose tolerance, with the K_i, Glc of H229S nearly doubling compared to the wild-type enzyme (Goswami et al., 2021). In my study, I experimentally determined the inhibition constant of glucose for the H229S variant to assess whether this enhanced tolerance could be replicated and quantitatively compared under our assay conditions.

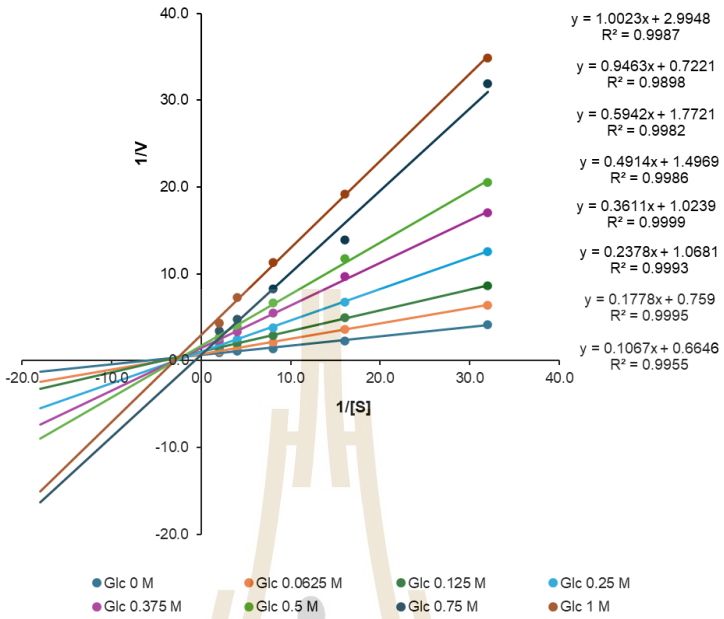

Figure 4.8 The Lineweaver-Burk plots of AtBGL5-H229S in the presence of different concentrations of glucose. The inverse of the initial rate (1/v0) is plotted against the inverse of the pNPGlc substrate concentration (1/[substrate] at different glucose concentrations.

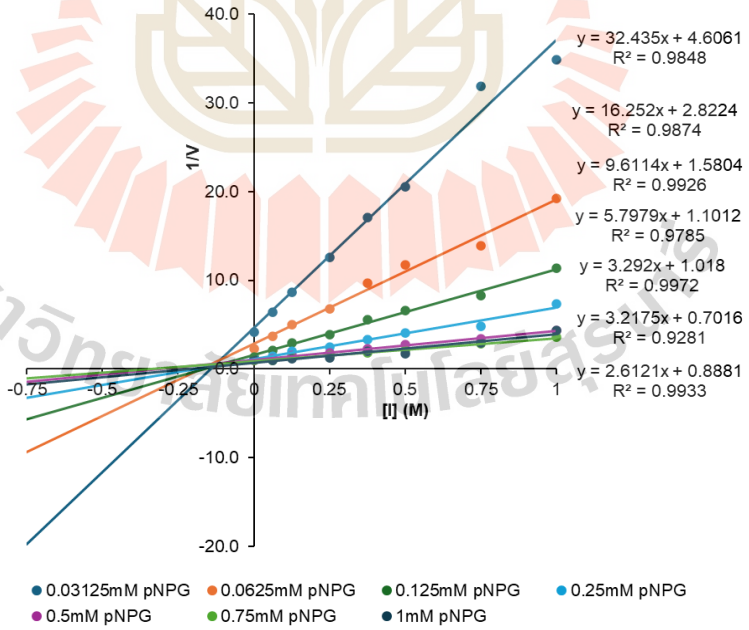

Figure 4.9 The Dixon plot of AtBGL5 inhibition by glucose. The inverse of the initial rate ($1/v_0$) is plotted against the concentration of inhibitor (glucose).

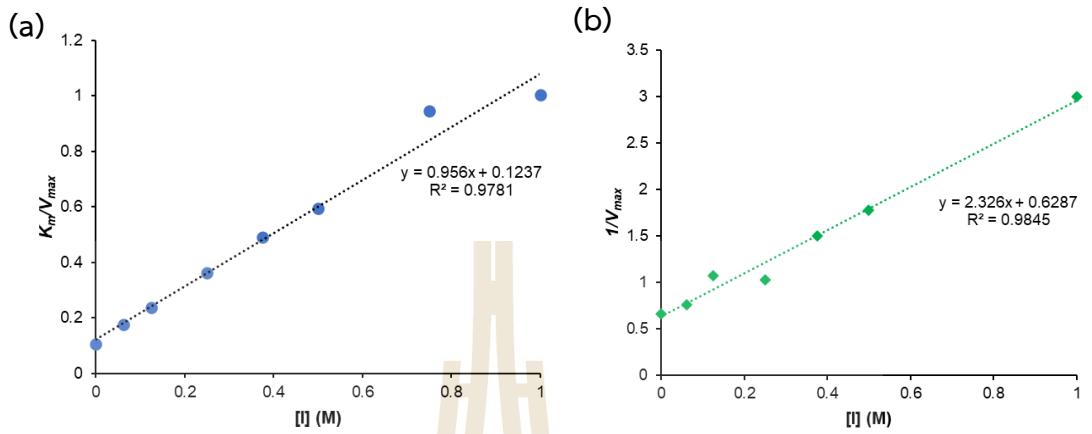

Figure 4.10 The derivative plot of AtBGL5-H229S inhibition by glucose. a) The Michaelis-Menten constant (K_m) divided by the maximum velocity (V_{max}) is plotted against the concentration of inhibitor (glucose). and (b) the inverse of the maximum velocity ($1/V_{max}$) is plotted against the concentration of inhibitor (glucose).

Table 4.4 The inhibition constant for AtBGL-H229S is obtained from the derivative plot, Figure 4.12.a for the competitive inhibition constant (K_{ic}) and Figure 4.12b for the uncompetitive inhibition constant (K_{iu}).

Inhibition constant	Value (mM)
competitive (K_{ic})	129 ± 31
uncompetitive (K_{iu})	270 ± 26

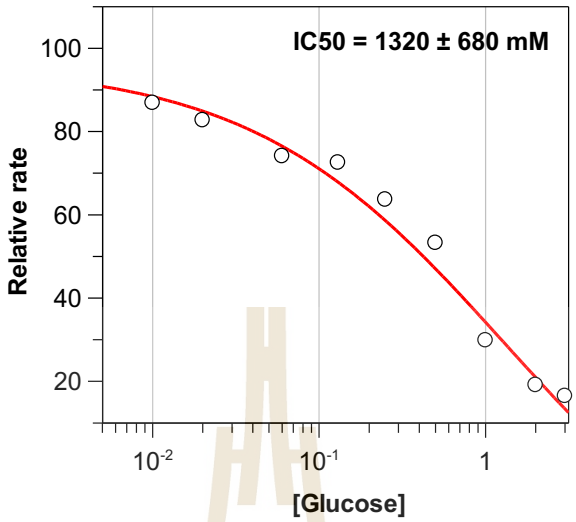

Figure 4.11 The 50% inhibitory concentrations (IC50) of glucose for the AtBGL5-H229S. The assay was performed at a fixed pNPGlc concentration of 1 mM, with glucose concentrations ranging up to 3 M.

The inhibition kinetics of the H229S mutant demonstrate a marked improvement in glucose tolerance compared to the wild-type AtBGL5 and notably differ from the data reported by (Goswami et al., 2021). In their study, the apparent K_i for glucose inhibition of the H229S variant was reported to be 1520 mM, a roughly two-fold improvement over the wild-type value of 686 mM. In contrast, my data show a more detailed inhibition profile, with the H229S mutant exhibiting a mixed inhibition (Figure 4.8), with the competitive inhibition constant (K_{ic}) of 129 ± 31 mM and the uncompetitive constant (K_{iu}) of 270 ± 26 mM (Table 4.4), alongside an IC50 of 1320 ± 680 mM at 1 mM substrate. Although my IC_{50} value aligns reasonably with their reported K_i, the breakdown of inhibition modes provides a much clearer picture of the mutation's mechanistic impact. K_{ic} and K_{iu} are significantly elevated in H229S compared to the wild type, confirming that the mutation substantially weakens glucose binding affinity across both enzyme states. These findings support the hypothesis that His229 is involved in glucose interaction, possibly through hydrogen bonding at the substrate entry site, and its replacement with serine disrupts this interaction, thereby reducing product inhibition. Unlike the original report, which

presents a single K_i value without kinetic mechanism resolution, my results reveal that the H229S mutant achieves glucose tolerance not just through a shift in binding strength but by broadly decreasing inhibitory interactions at binding states. This mechanistic insight underscores the value of kinetic deconvolution in enzyme engineering studies and affirms the industrial relevance of H229S, particularly for applications operating under high-glucose concentrations.

Glucono-δ-lactone (GDL) inhibition

To further refine the integration of β-glucosidase and FAD-dependent glucose dehydrogenase (FAD-GDH) into a coherent biocatalytic system, it is essential to evaluate the potential inhibitory effects of glucono-δ-lactone (GDL) on β-glucosidase activity. Given that GDL is the immediate oxidation product of glucose via FAD-GDH, its accumulation poses a risk of feedback inhibition that could impair the upstream release of glucose from cellulose-derived oligosaccharides. This is particularly relevant for the β-glucosidase AtBGL5 from *Agrobacterium tumefaciens*, along with its engineered variant AtBGL5-H229S, both of which are key candidates for use in enzymatic cascade reactions. To assess GDL sensitivity, a *p*NPGlc-based colorimetric assay was employed, enabling real-time monitoring of β-glucosidase activity through p-nitrophenol release. Kinetic parameters were determined across a substrate concentration range of 0–1 mM *p*NPGlc, while GDL was introduced at incremental concentrations from 37.25 μM up to 2 mM, which was previously found to be optimal for observing inhibition without overwhelming the system. This approach allows for the characterization of the inhibition profile and, potentially, the mechanistic classification (e.g., competitive, uncompetitive) of GDL's interaction with the enzyme. Comparing the wild-type and mutant forms of AtBGL5 under these conditions offers valuable insight into how structural modifications affect resistance to feedback inhibition and, in turn, informs the rational pairing of enzymes in a cascade that must operate efficiently despite the dynamic buildup of reaction products.

AtBGL5

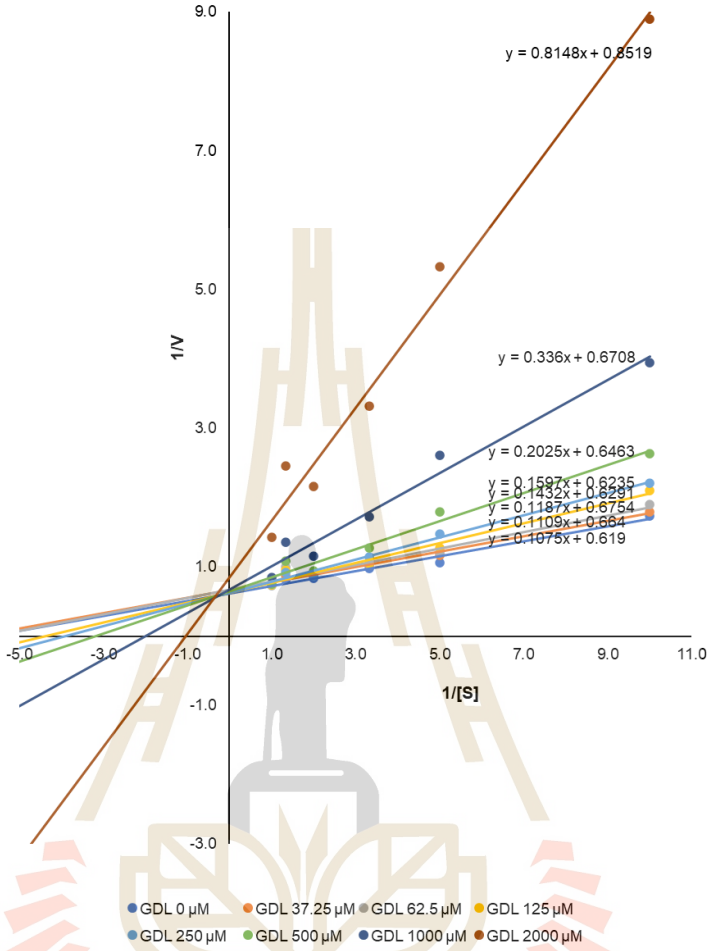

Figure 4.12 The Lineweaver-Burk plots of AtBGL5 in the presence of different concentrations of glucono-δ-lactone. The inverse of the initial rate ($1/v_0$) is plotted against the inverse of the pNPGlc substrate concentration (1/[substrate] at different substrate concentrations.

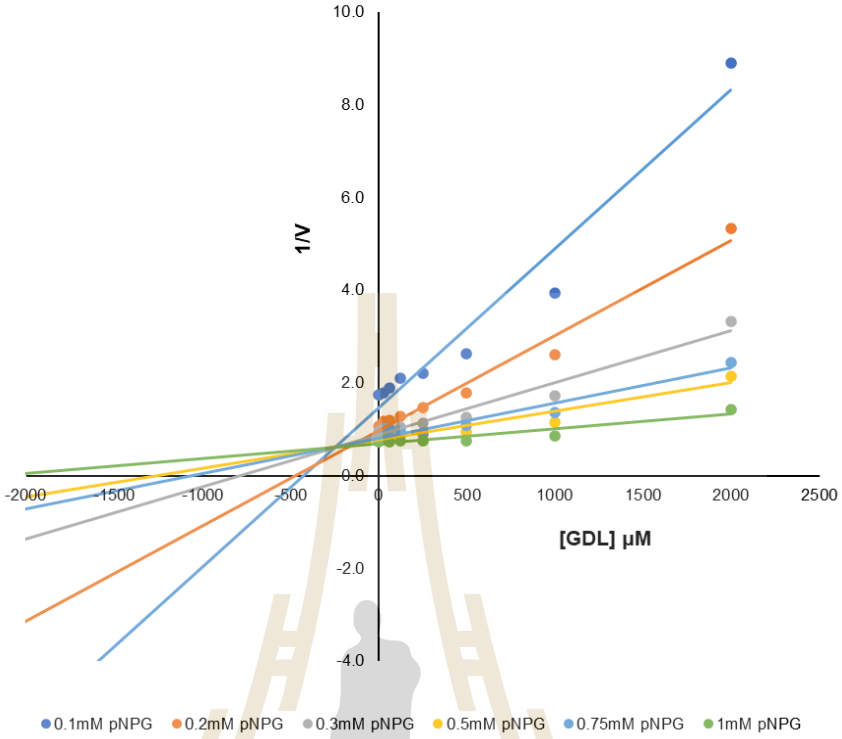

Figure 4.13 The Dixon plot of AtBGL5 inhibition by glucono-δ-lactone (GDL). The inverse of the initial rate ($1/v_0$) is plotted against the concentration of inhibitor (glucono-δ-lactone).

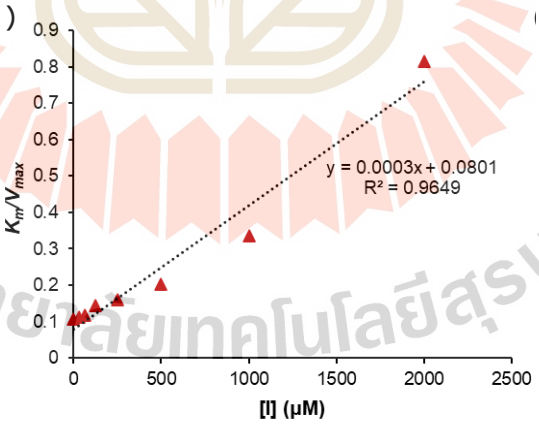

Figure 4.14 The derivative plot of AtBGL5 inhibition by glucono-δ-lactone.The Michaelis-Menten constant (K_m) / the maximum velocity (V_{max}) against the concentration of inhibitor (glucono-δ-lactone).

Table 4.5 The inhibition constant for AtBGL is obtained from the derivative plot for the competitive inhibition constant (K_{ic})

Inhibition constant	Value (μM)
competitive (K_{ic})	267 ± 72

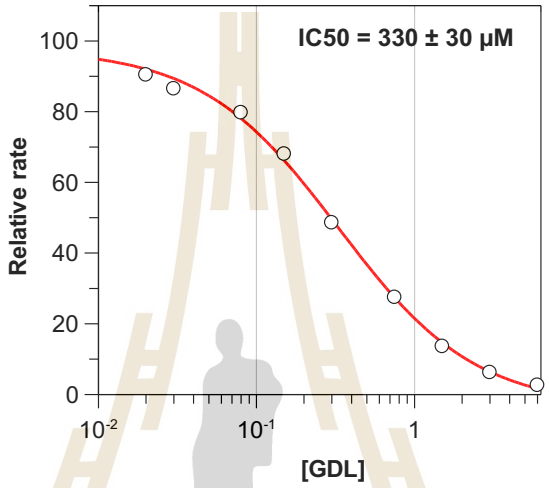

Figure 4.15 The 50% inhibitory concentrations (IC50) of glucono-δ-lactone for the AtBGL5. The assay was performed at a fixed pNPGlc concentration of 1 mM, with glucono-δ-lactone concentrations ranging up to 2 mM.

Kinetic analysis of glucono-δ-lactone (GDL) inhibition on wild-type AtBGL5 revealed essentially competitive inhibition, as supported by the linear curves that cross within error of the y-axis in the Lineweaver-Burk plot (Figure 4.12). The Dixon plot (Figure 4.13) shows the intercept at the K_{ic} to quantify this. This inhibition mode indicates that GDL interacts primarily with the free enzyme. Quantitatively, the competitive inhibition constant (K_{ic}) was determined to be 267 ± 72 μM. substantially lower than the uncompetitive constant (K_{iu} = 6440 ± 170 μM), further confirming the dominance of competitive binding (Table 4.5). The relatively low IC50 value of 330 ± 30 μM at 1 mM *p*NPGlc substrate corroborates the enzyme's sensitivity to GDL, even at modest concentrations that might be encountered in coupled systems where FAD-GDH generates this metabolite continuously. These findings highlight a critical

bottleneck in cascade design, where accumulation of GDL may transiently inhibit AtBGL5 and thereby limit the upstream release of glucose for further oxidation. Understanding this inhibitory behavior not only underscores the need for precise control of reaction conditions or potential GDL removal strategies but also provides a reference point for evaluating engineered variants with improved resistance to feedback inhibition.

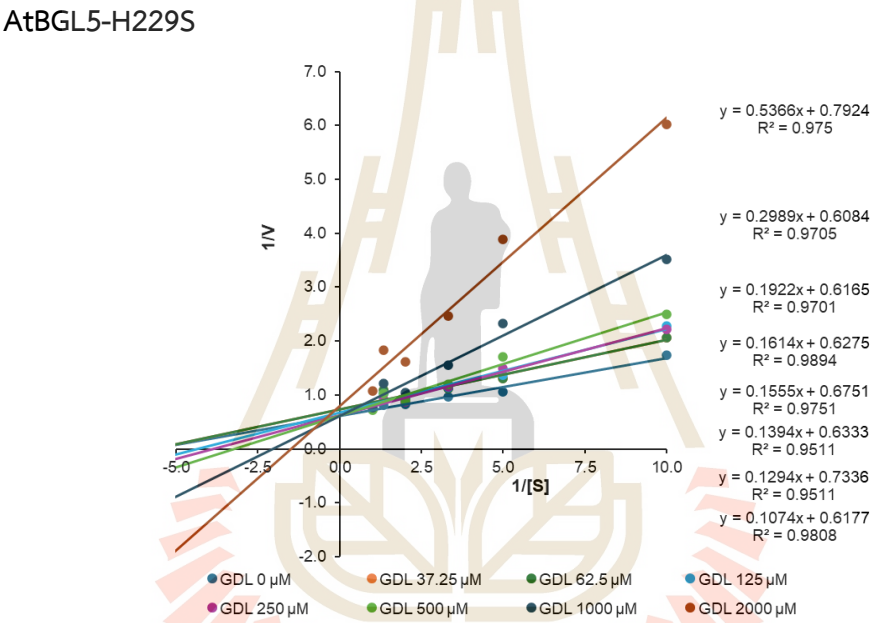

Figure 4.16 The Lineweaver-Burk plots of AtBGL5-H229S in the presence of different concentrations of glucono-δ-lactone. The inverse of the initial rate ($1/v_0$) is plotted against the inverse of the pNPGlc substrate concentration (1/[substrate] at different glucose concentrations.

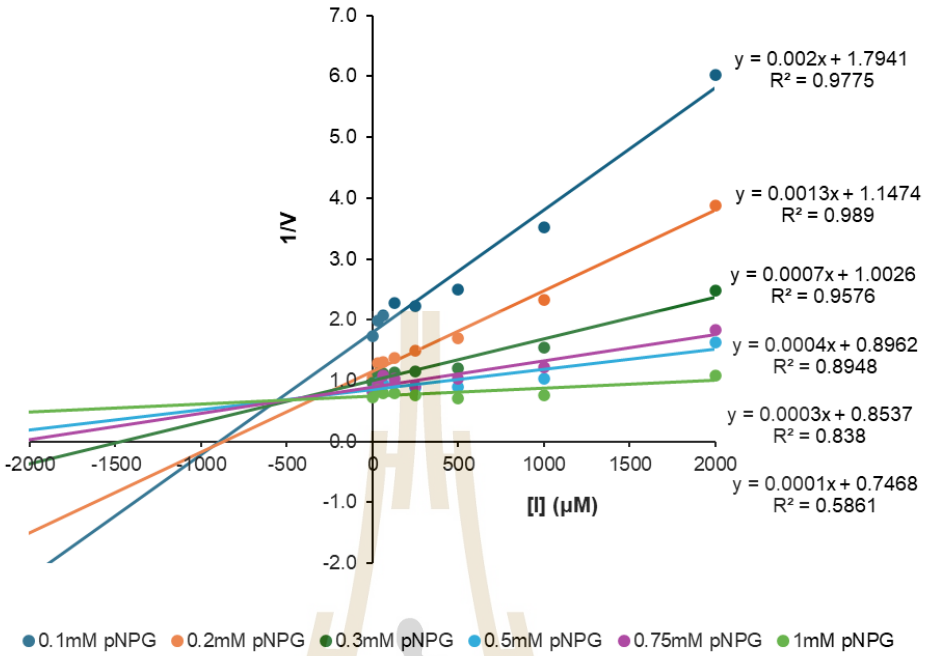

Figure 4.17 The Dixon plot of AtBGL5-H229S inhibition by glucono-δ-lactone (GDL). The inverse of the initial rate ($1/v_0$) is plotted against the concentration of inhibitor (glucono-δ-lactone).

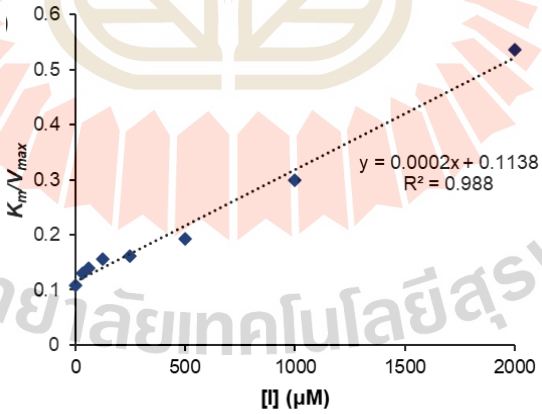

Figure 4.18 The derivative plot of AtBGL5-H229S inhibition by glucono-δ-lactone. The Michaelis-Menten constant (K_m) / the maximum velocity (V_{max}) against the concentration of inhibitor (glucono-δ-lactone).

Table 4.6 The inhibition constant for AtBGL-H229S is obtained from the derivative plot for the competitive inhibition constant (K_{ic})

Inhibition constant	Value (μM)
competitive (K_{ic})	570 ± 140

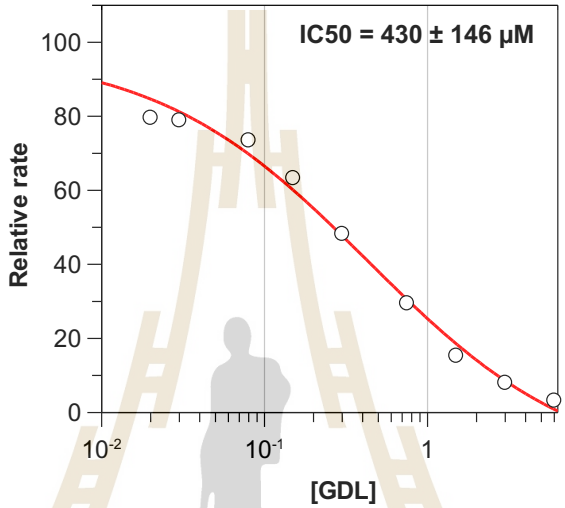

Figure 4.19 The 50% inhibitory concentrations (IC50) of glucono-δ-lactone for the AtBGL5. The assay was performed at a fixed pNPGlc concentration of 1 mM, with glucono-δ-lactone concentrations ranging up to 2 mM.

The AtBGL5-H229S variant, engineered to modulate catalytic or regulatory properties, similarly exhibited predominantly competitive inhibition by glucono-δ-lactone, as evidenced by Lineweaver-Burk curves intersecting within error of the y-axis (Figure 4.16). However, the inhibition constants showed a noticeable shift compared to the wild type. The competitive inhibition constant (K_{ic}) increased to 569 ± 38 μM, more than double that of the native enzyme, indicating a reduced overall affinity of the inhibitor for the enzyme. This attenuation in GDL binding is further reflected in the higher IC_{50} value of 430 ± 146 μM (Figure 4.19), suggesting a modest but functionally significant improvement in resistance to feedback inhibition by the GlcDH product. These results imply that the H229S mutation, although not eliminating GDL sensitivity, may confer a more permissive kinetic profile under product-accumulating conditions,

thus supporting greater stability of catalytic throughput when coupled with FAD-GDH. This subtle shift in inhibition dynamics might make AtBGL5-H229S a promising candidate for integration into enzyme cascades where product buildup, particularly if glucose or glucono-δ-lactone presents a challenge to sustained enzymatic performance.

4.4 Electrochemical characterization

This work presents a bi-enzymatic cascade bioanode system designed for the electrochemical oxidation of cellulose-derived oligosaccharides, with a particular focus on cellobiose, a disaccharide composed of two β-1,4-linked glucose units and a key intermediate in the enzymatic hydrolysis of cellulose. As cellobiose can be directly oxidized electrochemically but with less benefit, a two-step enzymatic strategy was employed to convert it into electroactive products. In the first step, β-glucosidase (AtBGL5) from *Agrobacterium tumefaciens* hydrolyzes the β-1,4 glycosidic linkage of cellobiose, liberating D-glucose. The resulting glucose is then oxidized by a high-performance FAD-dependent glucose dehydrogenase (FAD-GDH) derived from *Talaromyces emersonii*, generating gluconolactone and transferring electrons via a polyethylenimine-ferrocene (PEI-Fc) redox polymer. The enzymatic and redox reactions involved in cellobiose hydrolysis and glucose oxidation, using ferrocene (Fc) units as mediators, are shown in Scheme 1. To construct the BFC, the bioanode is connected to the horseradish peroxidase (HRP)-based biocathode, which catalyzes the reduction of hydrogen peroxide (H_2O_2) to water. As shown in Scheme 2.

$$n\text{Cellobiose} + \text{AtBGL5 or AtBGL5-H229S} \longrightarrow n\text{Glucose} \quad (1)$$

$$n\text{Glucose} + \text{TeGlcDH(FAD)} \longrightarrow n\text{Glucono-}\delta\text{-lactone} + \text{TeGlcDH}(FADH_2) \quad (2)$$

$$\text{TeGlcDH}(FADH_2) + 2Fc^{+} \longrightarrow \text{TeGlcDH(FAD)} + 2H^{+} + 2Fc \quad (3)$$

Scheme 1. The reaction scheme of the bioanode

$$H_2O_2 + \text{HRP[Fe(III)]} \longrightarrow H_2O + \text{HRP(C-I)} \quad (1)$$

$$\text{HRP(C-I)} + e^{-} + H^{+} \longrightarrow \text{HRP(C-II)} \quad (2)$$

$$\text{HRP(C-II)} + e^{-} + H^{+} \longrightarrow \text{HRP[Fe(III)]} + H_2O \quad (3)$$

Scheme 2. The reaction scheme of the biocathode peroxidase cycle of horseradish peroxidase enzymes (HRP). C-I and C-II refer to the compound I and compound II intermediates in the HRP peroxidase catalytic cycle.

Bioanode

To construct the bioanode, a graphene-based screen-printed electrode (SPE) with a 3 mm diameter surface was used due to its excellent electrical conductivity and high surface area, which provided enhanced current response during initial screening compared to traditional carbon electrodes. The bioanode design was aimed at enabling electrochemical oxidation of glucose derived from the enzymatic hydrolysis of cellulose-derived oligosaccharides such as cellobiose

The catalytic system integrates a cascade of enzymatic reaction. First, β-glucosidase (AtBGL5) from *Agrobacterium tumefaciens* hydrolyzes cellobiose into glucose. The resulting glucose is then oxidized by FAD-dependent glucose dehydrogenase (FAD-GDH) from *Talaromyces emersonii*. This oxidation produces gluconolactone, a valuable chemical intermediate, while releasing electrons for current generation. Although FAD-GDH initially appeared to have potential for direct electron transfer (DET), preliminary electrochemical measurements indicated that DET was inefficient. (Figure A.3). Therefore, a mediated electron transfer (MET) approach was adopted using a polyethylenimine-ferrocene (PEI-Fc) redox polymer as the

electron shuttle. This mediator facilitated efficient electron transfer from the FAD-GDH active site to the electrode surface. In early optimization studies, both the wild-type β-glucosidase (AtBGL5) and its glucose-tolerant H229S mutant were evaluated. Interestingly, the wild-type consistently yielded higher catalytic currents in cyclic voltammetry. Although the H229S variant is designed to resist glucose inhibition, the wild-type AtBGL5 possesses approximately 20% higher V_{max}, which appears to enhance catalytic turnover under the conditions tested. Since glucose inhibition becomes significant only at sustained high concentrations, the short reaction time and localized nature of the substrate application (70 µL of 100 mM cellobiose drop-cast directly on the electrode during the measurement) likely prevented inhibitory glucose buildup. Thus, the wild-type enzyme was selected for all subsequent experiments due to its superior current response in this bioelectrocatalytic activity.

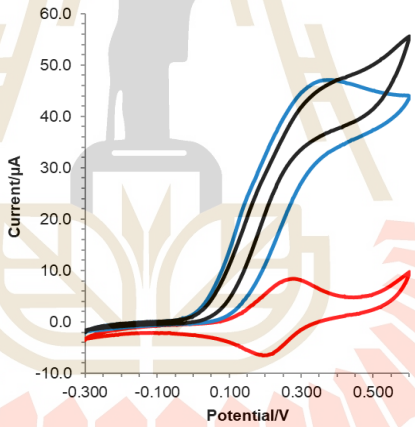

Figure 4.20 The cyclic voltammogram for the bioanode; the optimum condition is AtBGL5 : TeGlcDH 91.67:18.33 µg (5:1), PEI-Fc 80 µg (2x), PEGDGE 21 mcg (1x) in the absence of substrate (red), in the presence of 100 mM cellobiose (blue) and in the presence of 200 mM glucose recorded at 37 °C with the scan rate 5 mVs^{-1} on the graphene electrode surface.

The catalytic behavior of the bioanode comprising AtBGL5 wild-type and TeGlcDH was evaluated via cyclic voltammetry (CV) under optimized loading conditions (91.67 µg AtBGL5 : 18.33 µg TeGlcDH), using PEI-ferrocene (PEI-Fc) and PEGDGE as crosslinking agents. The measurements were carried out at 37 °C with a

scan rate of 5 mV s^{-1} on a graphene-modified electrode, as shown in Figure 4.20. A distinct catalytic current was observed upon glucose addition, indicating effective electron transfer from glucose oxidation through the enzyme cascade to the electrode surface. The onset potential for catalysis was approximately -40 mV, which aligns with the expected redox activity of the Fc-mediated system. The use of PEI-Fc on graphene provided a favorable electronic interface and high enzyme immobilization efficiency, attributable to the large surface area and π-π stacking interactions inherent to graphene. The shape of the voltammogram and the position of the anodic peak suggest that the ferrocene moieties within the PEI polymer acted as effective redox mediators, facilitating rapid electron shuttling. The observed current enhancement confirms that the enzymatic cascade, comprising cellulose-derived glucose hydrolysis by AtBGL5 and subsequent oxidation by TeGlcDH, is functionally coupled and electrochemically responsive. These results validate the feasibility of this bioanode design for downstream application in biofuel cells or biosensing platforms.

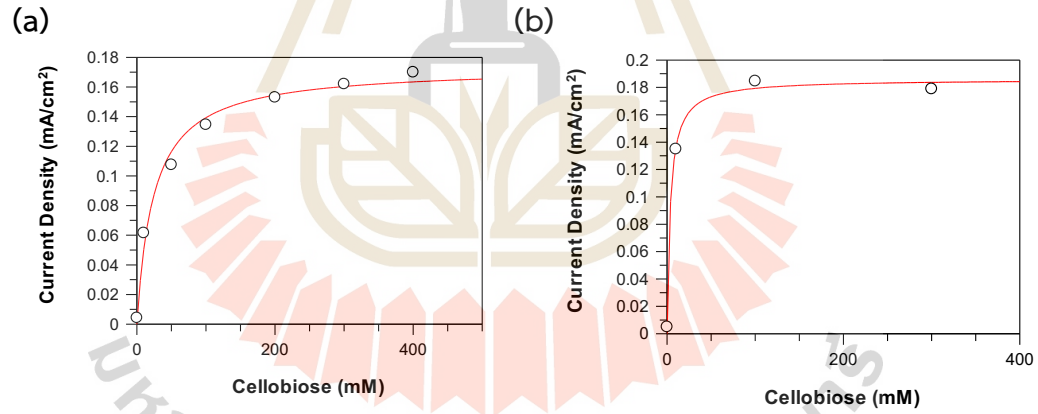

Figure 4.21 The apparent kinetic parameter determination on cellobiose concentration for the two immobilization techniques, two-layer immobilization (a) and co-immobilization (b), was performed by chronoamperometry.

Table 4.7 The apparent Michaelis-Menten parameters for two immobilization techniques.

Parameter	2-Layers immobilization	Co-immobilization
K_m^{app} (mM)	24.5 ± 4.6	3.71 ± 0.76

In enzymatic bioelectrocatalysis, the apparent Michaelis–Menten constant (K_m) is often used to assess the affinity of an immobilized enzyme system toward its substrate. When applied to bioelectrodes, an apparent K_m can be determined from the current response as a function of substrate concentration, reflecting not only the enzyme's intrinsic activity but also how effectively the immobilized system facilitates substrate access and catalytic turnover. In this study (Figure 4.21), two immobilization strategies were compared for a cascade bioanode comprising β-glucosidase (AtBGL5) and FAD-dependent glucose dehydrogenase (FAD-GDH): a two-layer immobilization, in which FAD-GDH was first deposited directly on the electrode followed by AtBGL5 as a top layer, and a co-immobilization approach, where both enzymes were mixed and drop-cast simultaneously. The co-immobilized system yielded a significantly lower apparent K_m of 3.71 ± 0.76 mM, compared to 24.5 ± 4.6 mM for the two-layer setup (Table 4.7). This suggests that co-immobilization promotes more efficient substrate channeling and reduces diffusional limitations between the hydrolytic and oxidative steps of the cascade. In contrast, the layered configuration may have introduced spatial separation or limited glucose diffusion between enzyme layers, resulting in a reduced catalytic efficiency. These findings underscore the importance of enzyme spatial arrangement in multi-enzyme electrode assemblies and support co-immobilization as a more effective strategy for cascade-driven bioelectrocatalytic systems.

Biocathode

The optimized HRP-based biocathode, constructed on a polyimide-graphene working electrode with 100 µg of horseradish peroxidase and 1 mM AzBTS as a diffusional redox mediator, demonstrated a cathodic current of approximately –0.2 mA under operational conditions (pH 6.0, 100 mM phosphate buffer, 150 mM NaCl, 37 °C) (Figure 4.26). This current represents the electrocatalytic activity of the cathode for the reduction of hydrogen peroxide to water, mediated efficiently by AzBTS. When connected to the corresponding enzymatic bioanode, this cathodic current defines the maximum rate at which the cathode can accept electrons under the given conditions, effectively acting as the upper limit for current output in the complete biofuel cell system. The magnitude of this cathodic current indicates that the HRP/AzBTS system is functioning efficiently, but also reveals that the biocathode may serve as the rate-limiting component if the bioanode can deliver higher currents. Thus, the cathode's ability to handle –0.2 mA becomes a critical factor in the overall performance of the biofuel cell. Further enhancement may be achievable by optimizing factors such as enzyme loading, mediator concentration, or electrode architecture to improve mediator diffusion and electron transfer kinetics. These results emphasize the importance of carefully balancing the electrocatalytic capacities of both anodic and cathodic components in a cascade-integrated bioelectrochemical system.

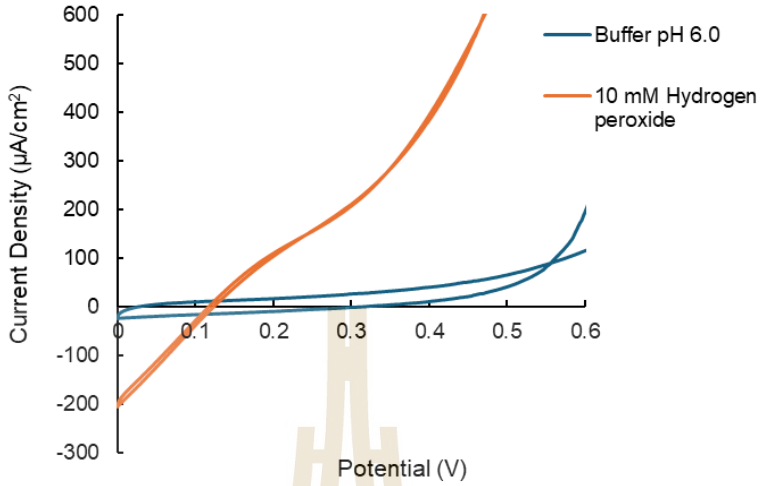

Figure 4.22 The cyclic voltammogram for the optimized biocathode: HRP 100 μg, 100 mM sodium phosphate buffer, 150 mM NaCl, pH 6.0, 37°C, 1 mM AzBTS (as diffuse mediator for HRP) on a 9 mm-diameter polyimide-graphene crafted working electrode.

The Biomass Fuel Cell

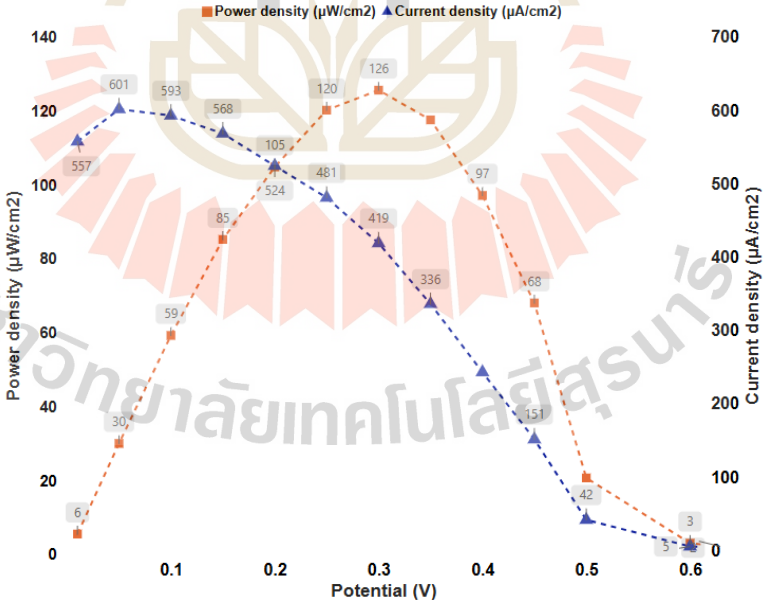

Figure 4.23 The polarization curve and power density curve of the biomass fuel cell in the cellobiose solution with the wild-type β-Glucosidase.

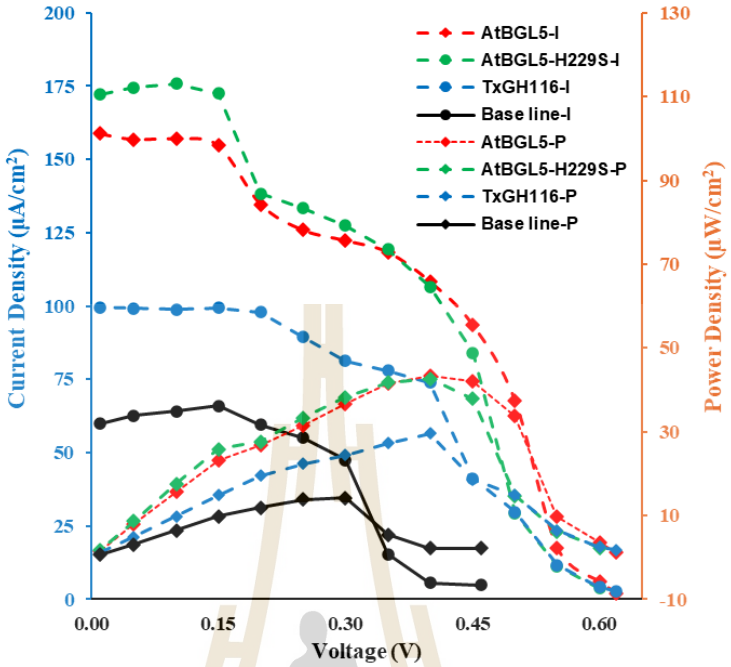

Figure 4.24 The Polarization curve and power density curve for the Biomass fuel cell (sugarcane leaves) with the different type of the β-glucosidases.

While initial experiments with co-immobilized AtBGL5 and FAD-GDH demonstrated promising electrocatalytic behavior, further optimization revealed that the β-glucosidase (AtBGL5) exhibited significantly higher catalytic efficiency when operating in solution rather than in an immobilized state. This observation is likely due to enhanced substrate accessibility and enzyme mobility in the bulk phase, which supports more effective hydrolysis of cellobiose into glucose, the actual substrate for FAD-dependent glucose dehydrogenase (FAD-GDH). As a result, the final configuration employed a selective immobilization approach, in which only FAD-GDH was immobilized on the graphene electrode surface, while AtBGL5 was supplied in the reaction medium. To ensure sufficient substrate turnover, the reaction was conducted in 20 mL of 100 mM cellobiose, while the electrochemical testing of the anode was performed with a drop of 70 μL of this solution applied directly onto the electrode surface. This hybrid system—combining an immobilized redox enzyme with a freely diffusing hydrolytic enzyme—proved to be highly effective. When integrated with the optimized HRP-based biocathode, the full enzymatic biofuel cell (Figure 4.23)

generated a stable open circuit voltage (OCV) of 0.6 V, a value consistent with efficient redox coupling between the cascade bioanode and the peroxide-reducing cathode. The maximum power density reached 126 μW/cm², and the peak current density was 0.6 mA/cm², With the real Biomass (sugarcane leaves) the results show the similar polarization and power density curve both wild-type AtBGL, AtBGL-H229 and the gluconolactone insensitive β-glucosidase (TxGH116) from our previous study slightly lower than the recent study, reflecting catalytic synergy between the enzymatic cascade and the redox mediation system. These results highlight the importance of spatial and functional separation in multi-enzyme systems, where allowing key steps, such as glycosidic bond cleavage, to occur in solution can unlock higher performance by relieving diffusional and structural constraints inherent to solid-phase immobilization. Overall, this approach offers a flexible and scalable strategy for enhancing the bioelectrocatalytic conversion of cellobiose in enzymatic biofuel cell platforms.

4.5 References

Goswami, S., Manna, B., Chattopadhyay, K., Ghosh, A., and Datta, S. (2021). Role of Conformational Change and Glucose Binding Sites in the Enhanced Glucose Tolerance of *Agrobacterium tumefaciens 5A* GH1 β-Glucosidase Mutants. *The Journal of Physical Chemistry B*, *125*(33), 9402–9416.

Okuda-Shimazaki, J., Yoshida, H., and Sode, K. (2020). FAD dependent glucose dehydrogenases—Discovery and engineering of representative glucose sensing enzymes. *Bioelectrochemistry (Amsterdam, Netherlands)*, *132*, 107414.

CHAPTER V
CONCLUSION

This study presents an integrated exploration of enzymatic function and applications, offering both mechanistic and practical insights into the behavior of *Agrobacterium tumefaciens* β-glucosidase (AtBGL5) and its H229S mutant, as well as TeGlcDH. Through detailed inhibition kinetics and bioelectrocatalytic system testing, we have demonstrated that the histidine residue at position 229 plays a structurally critical role in stabilizing the active site conformation that enables effective glucose binding. While Goswami et al. (2021) previously reported an apparent K_i of 686 mM for the wild-type and 1520 mM for the H229S mutant, our analysis revealed significantly stronger inhibition by glucose in the wild-type enzyme, with a K_{ic} of 75 ± 11 mM and an IC_{50} of 94 ± 38 mM, indicating that glucose acts as a stronger mixed inhibitor than expected from the literature. In contrast, the H229S variant exhibited a marked reduction in glucose sensitivity, with a K_{ic} of 145 ± 12 mM and an IC_{50} of 1320 ± 680 mM, aligning qualitatively with the prior report's conclusion that the mutation confers improved glucose tolerance. Importantly, our findings extend the molecular interpretation offered by Goswami et al. by showing that His229 likely does not directly participate in glucose binding but rather maintains the structural integrity necessary for productive inhibitory interactions at the active site.

This hypothesis is supported by the retained but slightly diminished inhibition of the AtBGL5 H229S variant by glucono-δ-lactone (GDL), a transition-state analog, which highlights the broader interaction profile of true transition-state inhibitors versus competitive ones like glucose. GDL acted as a competitive inhibitor, with K_{ic} values of 267 ± 72 μM for AtBGL5 and 570 ± 140 μM for AtBGL5 H229S. Due to the production of GDL by TeGlcDH, this inhibition may significantly impact the biofuel output if GDL is not hydrolyzed to gluconic acid rapidly enough.

These biochemical findings had direct implications for our bioelectrocatalytic application. While the H229S mutant displayed reduced inhibition and thus would be presumed advantageous under product-accumulating conditions, its overall catalytic performance in the electrochemical system was inferior to the wild-type enzyme, probably due to its lower V_{max} and catalytic turnover under our operational timescale. These results emphasize a crucial nuance: improved glucose tolerance does not necessarily translate to enhanced performance in short-timescale, low-glucose-load systems like our enzymatic biofuel cell. Consequently, we opted for the wild-type AtBGL5 in our final bi-enzymatic cascade with FAD-dependent glucose dehydrogenase (TeGlcDH).

Furthermore, our experimentation with enzyme immobilization revealed that AtBGL5 performs more efficiently in solution, where it retains conformational mobility, as opposed to being surface-tethered, which likely impedes its structural dynamics or diffusion of substrate to the active sites of the two enzymes. This insight was central to the final architecture of our biofuel cell, which achieved robust electrocatalytic activity and efficient biomass-to-energy conversion, delivering a maximum power density of 126 μW/cm² and an open circuit voltage of 0.6 V.

In summary, this work substantiates and expands on the conclusions of Goswami et al. by offering higher-resolution kinetic data, contextualizing the functional role of His229 in both structural and applied terms, and demonstrating how mechanistic enzymology can directly inform practical design choices in bioelectrochemical systems. It reinforces the importance of kinetic dissection in enzyme engineering, showing that rationally designed mutations like H229S can alleviate product inhibition but that their performance must still be evaluated holistically within specific application frameworks. The integration of fundamental structure-function analysis with device-level optimization not only enables the development of tailored enzymatic components but also lays the groundwork for more efficient, renewable energy systems derived from lignocellulosic biomass.

APPENDIX

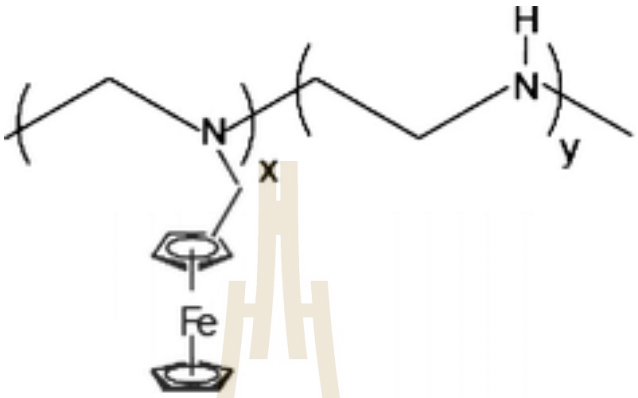

Figure A.1 Structure of Linearized-Poly(ethylenimine)-Ferrocene (LPEI-Fc).

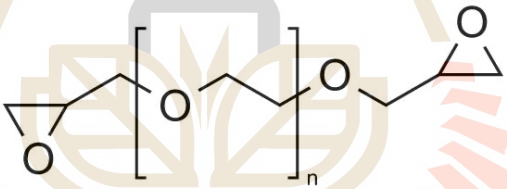

Figure A.2 Structure of Poly(ethylene glycol) diglycidyl ether (PEGDGE).

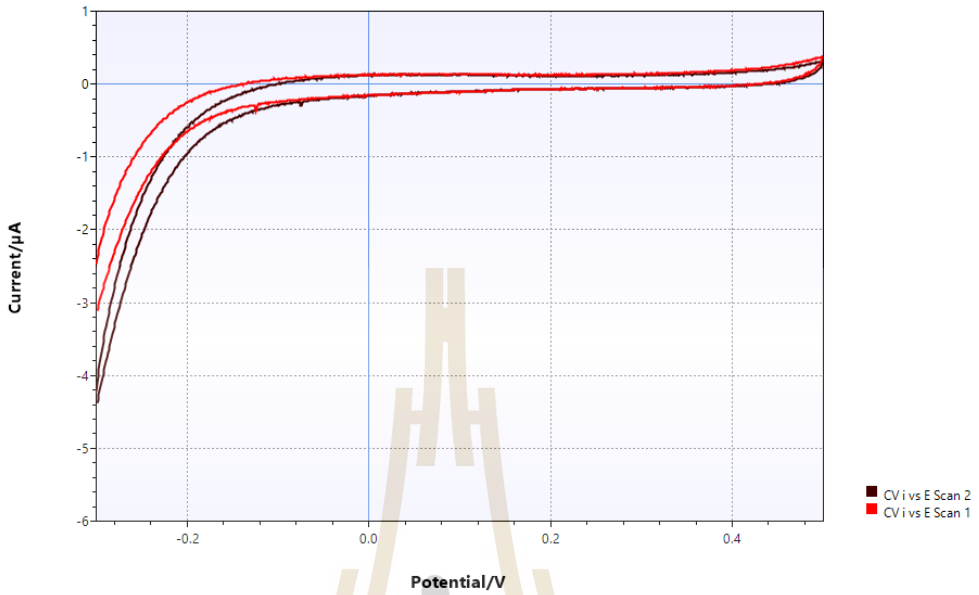

Figure A.3 The preliminary result of Cyclic voltammogram for testing the direct electron transfer (DET) properties of FAD-Glucose dehydrogenase.

CURRICULUM VITAE

NAME	Mr. Luciranon Sribrahma
DATE OF BIRTH	August 26, 1999
PLACE OF BIRTH	Nakhon Ratchasima, Thailand
EMAIL	M6500733@g.sut.ac.th

EDUCATION

2022 - 2024	**Master of Science (M.Sc.)** in Biochemistry and Biochemical Technology, Suranaree University of Technology, Nakhon Ratchasima, Thailand.
2018 - 2022	**Bachelor of Science (B.Sc.)** in Chemistry, Suranaree University of Technology, Nakhon Ratchasima, Thailand.

Work Experience

- At Biochemistry Laboratory (Suranaree University of Technology, Thailand).
  Worked as a teaching assistant. (2023-2024)

Conferences/Presentation

Luciranon Sribrahma, Chamaipon Beagbandee, James R. Ketudat-Cairns, Piyanut Pinyou, Engineered-Enzyme Biomass Fuel Cells: Enhancing Bio-electrochemical Efficiency for Sustainable Energy. The 5th International Symposium on Frontiers in Molecular Science (ISFMS2025), 26–29 August 2025, Kyoto Institute, Library and Archives, Rekisaikan, Kyoto, Japan. Poster presentation (Best Poster Presentation Awarded)